



Universitetet
i Stavanger

FACULTY OF SCIENCE AND TECHNOLOGY

MASTER'S THESIS

Study programme/specialisation:

Engineering Structures and Materials
Mechanical systems

Spring semester, 2019

Open

Author:

Joakim Matthias Felix Fischer

Joakim Fischer

Programme coordinator: **Dimitrios Pavlou**

Supervisors: **Dimitrios Pavlou, Jørgen Apeland**

Title of master's thesis:

Structural Response Analysis of a Composite Multirotor Airframe

Credits: **30**

Keywords:

Multirotor airframe
Structural response
Finite element analysis
Composite materials

Number of pages: **53**

Stavanger, 2019-06-15

Structural Response Analysis of a Composite Multirotor Airframe

Joakim Fischer, MSc Student

Engineering Structures and Materials

Mechanical Systems

Department of Mechanical and Structural Engineering and Materials Science,
University of Stavanger

June, 2019



Abstract

In this work, finite element analyses determine the modal frequencies and relative stiffness of two multicopter airframes—the Camflight FX-8 and its water-resistant variant BG-200.

Details of the analysis procedure are included: Development of 3D models, definition of composite airframe materials, and setup of simulation cases. Future simulations are facilitated by describing the simulation workflow and identifying key considerations.

Static structural analyses indicate a substantial increase in stiffness from the FX-8 to BG-200 model, also represented in the modal simulations. Areas of stress concentration and critical components in both designs are identified for future studies. Overall results also form a basis for assessing future structural improvements; Some recommendations for such are also supplied.

Keywords: Multicopter airframe, Structural response, Finite element analysis, Composite materials

1 Acknowledgements

My heartfelt gratitude goes to Professor Dimitrios Pavlou for supervising both this thesis and the bachelor's thesis before it; His patience and academic advice have been invaluable. My second supervisor, Jørgen Apeland, deserves special thanks for his exemplary enthusiasm and professionalism when providing advice, encouragement and extensive feedback at every step of the journey.

Nordic Unmanned AS has been immensely helpful beyond originally proposing this thesis subject. The employees have been very welcoming, and especially accommodating regarding measurements, design files, and general information.

Finally, I would like to thank my parents for being wonderfully supportive in every way they can think of.

Contents

1	Acknowledgements	i
2	Introduction	1
2.1	Background	1
2.2	Scope	1
2.3	Prerequisite knowledge	2
2.4	Thesis structure	2
2.5	Camflight FX-8 and BG-200	4
3	General workflow	7
3.1	Geometry	10
3.2	Meshing	12
3.2.1	Element quality	12
3.2.2	Element type	13
3.2.3	Mesh refinement	15
3.3	Materials	16
3.4	Simulation setup	18
3.4.1	Modal	18
3.4.2	Static structural	19
4	Numerical Model	20
4.1	Geometry	20
4.1.1	3D model development	20
4.1.2	Simplifications	21
4.2	Meshing	23
4.2.1	Element quality	23
4.2.2	Element types	23
4.2.3	Mesh refinement	24
4.3	Materials	25
4.3.1	Isotropic materials	25
4.3.2	Composite materials	26
4.4	Modal analysis	30

4.5	Static structural analysis	31
5	Results	32
5.1	Modal analysis	33
5.1.1	Modal frequencies	33
5.1.2	Modal shapes	36
5.1.3	Effect of payloads	41
5.2	Static structural analysis	42
6	Discussion and conclusions	44
6.1	Validity	44
6.1.1	Effect of element type	45
6.1.2	Effect of element size	47
6.2	Goal achievement	49
6.2.1	Relative structural performance	49
6.2.2	Key workflow considerations	51
6.2.3	Critical components and improvements	52
6.3	Future opportunities	53

2 Introduction

2.1 Background

While the UAV industry has matured considerably since its explosive entry onto the market, leading companies are still stretching limits to gain a head start on the next innovation in a rapidly evolving field. Continuous improvements must be made quickly yet efficiently, or one falls behind the competition in performance or cost. Finite element simulations can be of great benefit during the design process when implemented correctly, potentially saving both economical and temporal resources.

Nordic Unmanned AS is the leading European provider of unmanned systems and services. One of their core products is the Camflight FX-8 drone, which sees extensive use within operations while providing a versatile platform for research and development.

Recently the company modified the staple FX-8 model to create a weather-resistant version named the BG-200. For the occasion they have invited the author, an MSc student from the University of Stavanger, to perform analyses on the two designs in hopes of better understanding the relative structural performance of the two designs.

2.2 Scope

At the core of this thesis is one research goal:

- Compare the structural performance of the FX-8 and BG-200 airframes.

Two sub-goals also emerge, primarily facilitating future work:

- Determine key considerations and good practices for the simulation process.
- Determine critical components and potential focal points for future improvements.

To achieve the above goals, the project is broken down into key tasks:

1. Perform finite element analysis
 - (a) Create numerical model
 - (b) Run modal and static structural analyses
2. Document workflow and good practice based on project experiences

Modal and static structural analyses determine the relative structural performance of the two designs. These do not consider wind or other dynamic loads, nor the harmonic response of the structures to such loads. Some simulations are run to determine good practices for airframe simulations, investigating how choice of finite element type as well as varying payloads can affect results. General notes on the simulation workflow are also included in their own section, while specific details for this thesis' simulations are kept separate.

The simulations provide better knowledge of the airframe structures and their relative performance, creating a basis for assessing future modifications. Future efforts to optimise the airframes may find both the results and the documented workflow to be useful.

2.3 Prerequisite knowledge

While most sections will have short explanations of some core concepts, it is assumed that the reader possesses a fundamental understanding of the thesis' core topics: Multirotors, finite element analysis, and fibre-reinforced composites' material science. Rudimentary familiarity with ANSYS Workbench and its component systems is also beneficial.

2.4 Thesis structure

After quickly formalising some terminology, the next section goes through the details of both the FX-8 and BG-200 drone airframes. This includes naming and comparing their primary components, as well as some overall drone specifications.

Section 3 presents the overall workflow of the entire project, providing some general

information of important considerations, and debates good practice for each step of the workflow. Specific details pertaining to this project's simulation setup are included in Section 4; It is again structured according to the workflow, with one section per step.

Simulation results are presented in Section 5. More qualitative results like the distribution of modal frequencies are initially interpreted here, while more substantial discussion and conclusions are contained in Section 6; This is where the structural performance of the airframes is compared, as well as discussions of critical components and potential for future improvements. Prospects for future research and improvements are also highlighted near the end.

2.5 Camflight FX-8 and BG-200

This thesis covers unmanned multirotors (also called multicopters), a subcategory of unmanned aerial vehicles (UAV), colloquially called drones. All terms may be used interchangeably in this thesis, but will all refer to multirotors. More specifically, the work in this thesis only covers the drone airframe, ignoring details of payloads, propulsion systems, and avionics unless they affect results in a significant manner.

Multicopter airframes have several functions. Chief among them is providing a frame for other components: Propulsion, batteries, payloads, and avionics. Other relevant features include landing gear and weatherproofing. There is a multitude of airframe designs, but the designs considered in this study are relatively simple variations of the bi-axial 8-motor X-configuration. Their core features are summarised by Figure 1 and 2.

The designs consist of two central plates (forming a hub providing room for electronics and connection points for payloads), tubular arms (booms) leading out to the propulsion system, landing gear, and a multitude of clamps which connect components. Figure 2 shows how the booms are connected to the plates in the centre as well as the simplified connectors (leg clamps) between legs and booms.

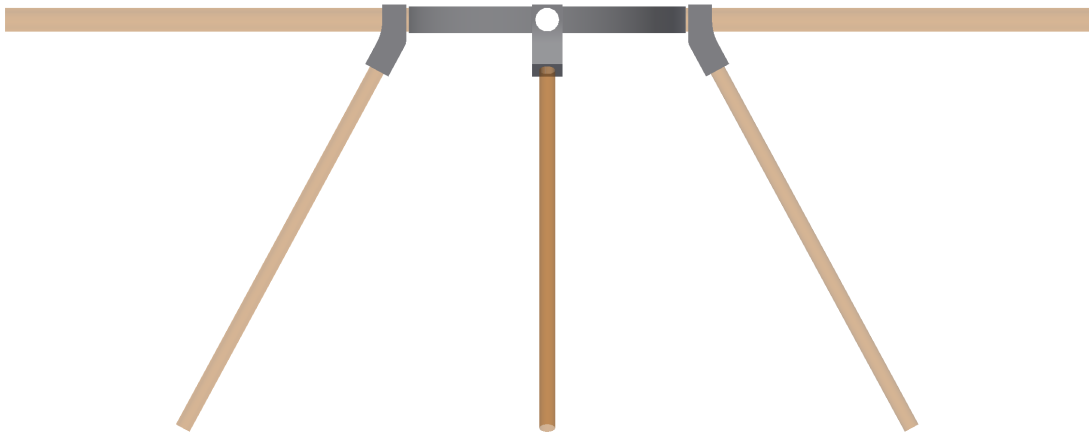


Figure 1: *Profile view of the BG-200 design. Carbon fibre components represented by translucent orange zero-thickness surfaces.*

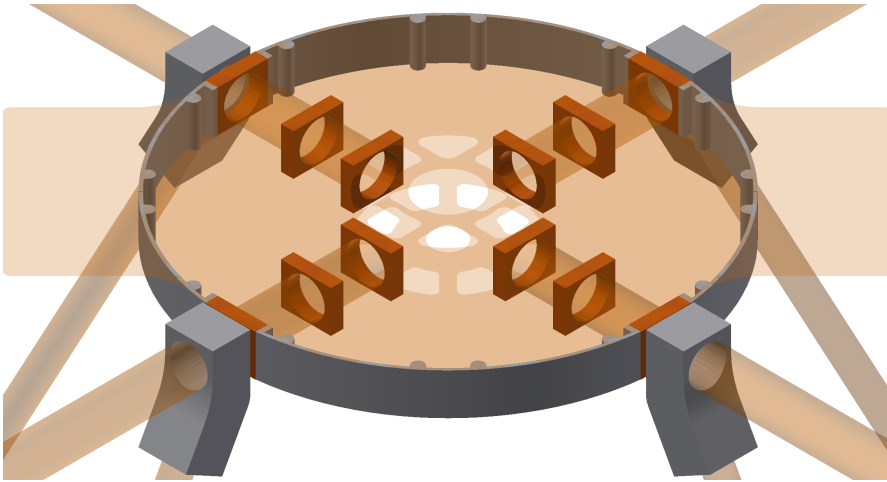


Figure 2: *Close-up view of the BG-200 centre. Clamps in deep orange, carbon fibre parts translucent orange, leg clamps and covers in grey.*

One key difference between designs is the covers; In the FX-8 design, these are replaced by cylindrical spacers placed along the circumference, overlapping the cylindrical protrusions of the covers at the midpoint between booms.

Although the covers are quite noticeable, the difference in plate design is even more so. Figure 3 shows the designs of the FX-8 and BG-200 plates. Note that the hole in the top BG-200 plate is there primarily for cable routing, and is covered by the avionics housing when in use. Batteries on this particular FX-8 plate design would not be fully contained on the solid area, being partially supported by the webbed rest of the plate.

To summarise: Both airframes consist of four booms, four landing gear legs, twelve clamps, four leg clamps, and two centre plates which differ between designs; The FX-8 plates are webbed to reduce weight, while the BG-200 plates are solid. Between the plates the FX-8 model features eight cylindrical spacers, while the BG-200 model has eight covers. Essentially, the FX-8 model is a lightweight alternative, but does not feature the same weather certifications; This work also aims to further nuance the comparison through structural response analysis.

General drone specifications are listed in Table 1.

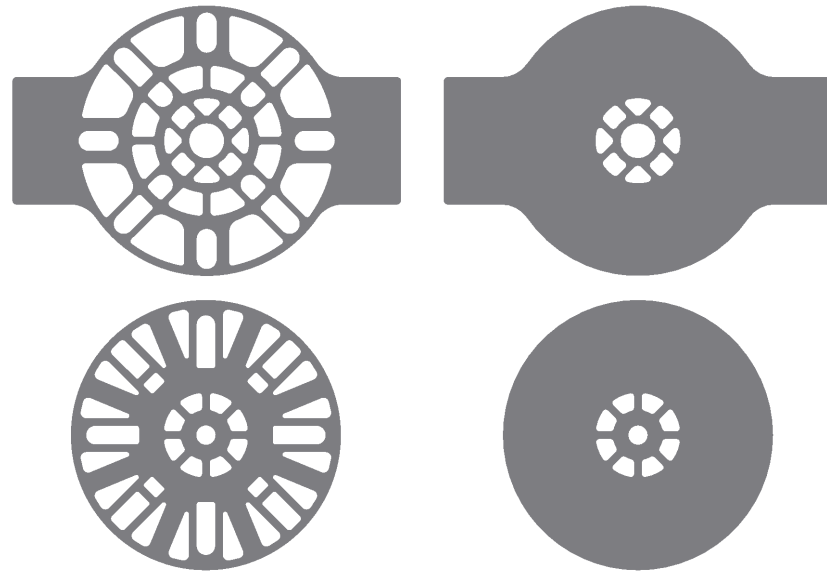


Figure 3: *Left: FX-8 plates. Right: BG-200 plates. Top plates along top row. Booms would lie in an X shape across each plate, batteries resting on the “flaps” of the top plates.*

Table 1: *General specifications of the drones. Weather-related statistics are inapplicable to the FX-8.*

Key specifications	
Max. take-off-weight	25 kg
Flight time (hover)	60 min
Max. speed	55 km/h
Max. payload capacity	10 kg
Max. wind	20 m/s
Dust and moisture	IP 55
Temperature range	-20–40 °C
Communication range	200 km
Energy supply	7.6 kg (Li-Po batteries)
Propulsion system	5.4 kg (8 Bi-axial)
Airframe mass	FX-8: 2.6 kg BG-200: 3.2 kg

3 General workflow

All simulations for this thesis were performed in ANSYS Workbench. It combines several of ANSYS' systems, like Fluent and Mechanical, creating cross-compatibility between the various tasks in a project. The primary interface of Workbench is based around the project workflow; This will be covered here to give an overview, as the rest of the thesis follows its structure. The Workbench project schematic is based on systems which in simple cases can be self-contained and in other cases interconnected.

Figure 4 shows the Workbench project schematic as shown in Workbench, and Figure 5 is an adaptation of the same workflow, with some keywords for each step. Note that some actions, like defining the masses of propulsion and batteries, can be done on several occasions but is only shown at the earliest possible point in the diagrams.

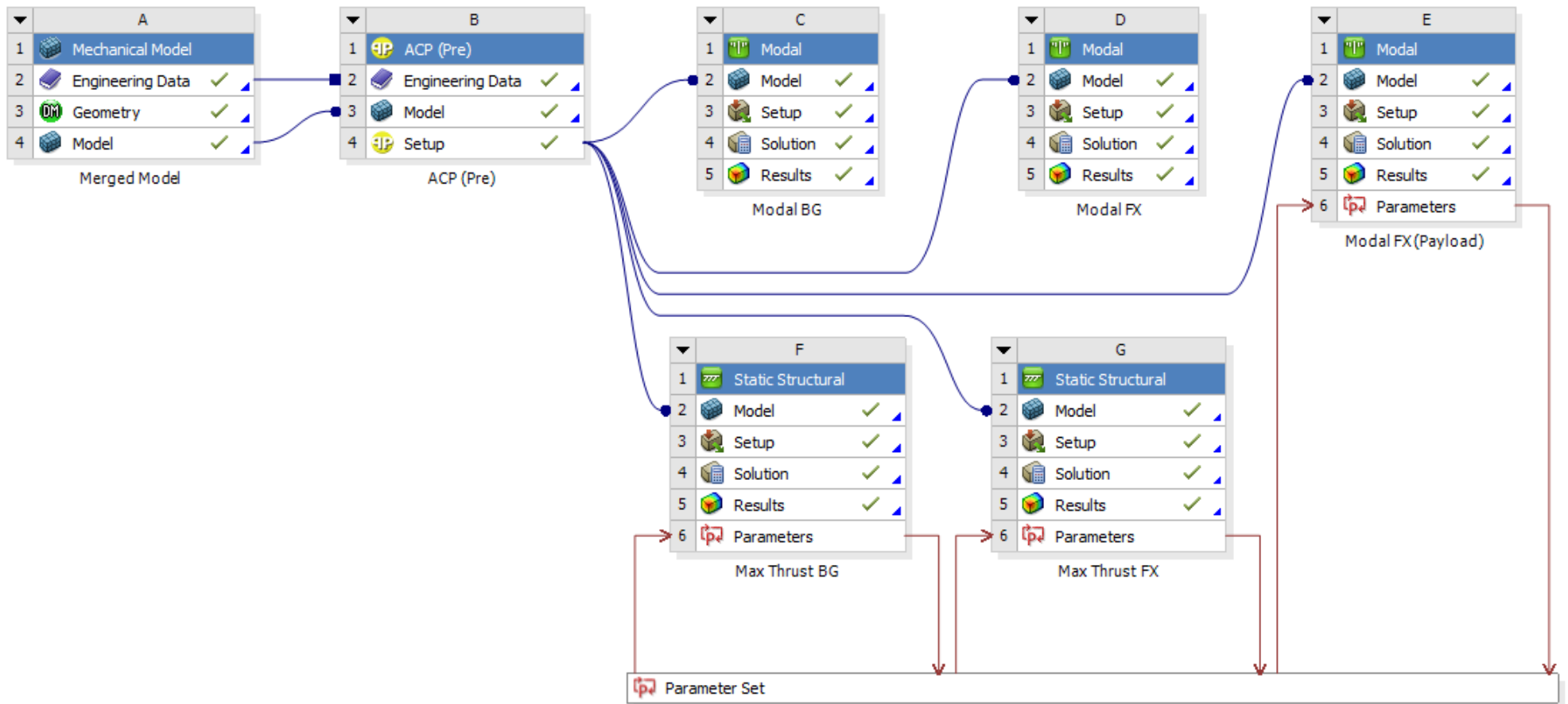


Figure 4: Project schematic from Workbench outlining the analysis structure.

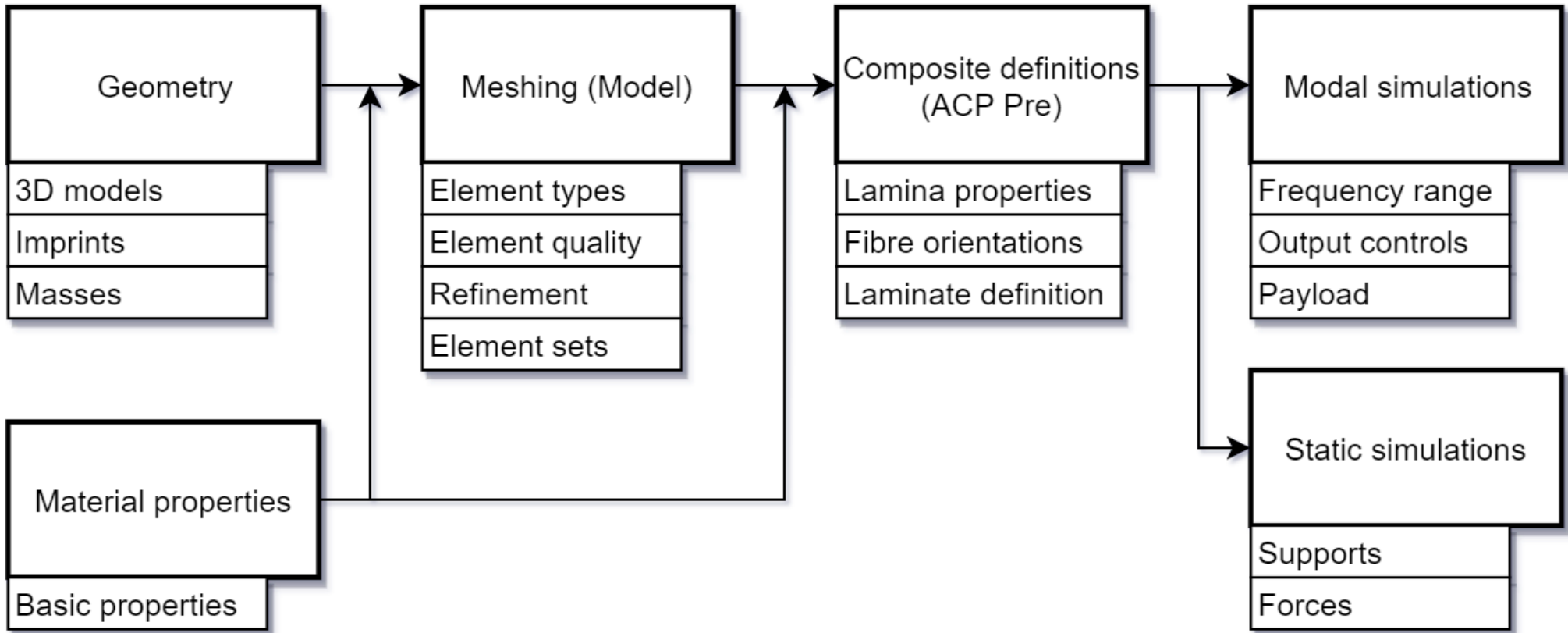


Figure 5: Abstracted workflow from project schematic, with added keywords.

Defining the geometry through 3D models is a core feature of modern finite element analysis, and forms the workflow's starting point. Once geometry has been defined, it can be meshed into finite elements. Incorporating carbon fibre in the simulations necessitates the ACP (ANSYS Composite PrepPost) system; This is where one defines fibre orientations, lamina stackups, and the like. These new material data are applied to the mesh elements and sent to the simulation environments. Each environment has different requirements for running a simulation: Modal simulations can be run with just a well-defined structure, while static structural analyses need information about supports and forces. Results, once properly verified, can then be put into use.

The following sections will provide general detail and key considerations for each of the previously mentioned steps, ordered according to the workflow shown in Figure 5.

3.1 Geometry

For a reasonably complex model like an airframe, geometry usually needs to be represented by a 3D model, assembled from models of each of its components. A multitude of software is capable of producing these models, but one should keep compatibility between modelling and simulation software in mind: A modelling program tailored for e.g. sculpting visual art may not have the same features as one made for mechanical engineering, which again might differ from structural engineering software. ANSYS of course attempts to work with engineering standard programs and file types.

Most standard modelling software supports both solid and surface modelling. When simulating composite materials with ACP, one needs to use surface bodies due to the layer-by-layer way ACP defines composite materials (see Section 3.3).

As is described in Section 4.1, it can be a natural during 3D model development to combine several designs into a single model, suppressing specific parts for specific simulations. This can streamline the workflow greatly, as one only needs to process a single geometry file (and much of the processing may be similar if one assesses

similar designs), but it carries some risk. Specifically for this project, the ACP system reset all suppression flags whenever it was run, meaning that each following system (all simulations) needed their suppression states redefined.

Further streamlining the workflow (especially regarding ACP), this thesis also used the same mesh for both static and structural analyses. This is inadvisable if performing absolute simulations and computational power is limited. For this relative analysis, absolute accuracy was not as vital, which made the streamlining technique more viable.

Another subject to keep in mind is the purpose of the model. In different types of simulations the importance of a component's level of detail can vary drastically. For example, accurately modelling the propulsion's propellers is of utmost importance in a fluid dynamics simulation (to e.g. evaluate thrust), but is unnecessary for analysing the strength of the airframe. Meanwhile, the propeller's vibration modes may again make it relevant for a modal analysis, if one desires such a level of detail.

Depending on simulation type and desired level of realism, one can perform various simplifications. Typically one would want to remove small details with low expected impact (fillet might for example appear to be a minor detail although it drastically affects stress concentrations depending on location). Beyond this, entirely removing a component and replacing it with a suitable boundary condition can also save simulation resources, e.g. by replacing the model of a spring with a spring-like element of proper stiffness, or removing a bolt model and simply assuming the bolted entities are bonded together. For an overview of simplifications used in this thesis, see Section 4.1.2.

3.2 Meshing

Once the geometric model has been thoroughly defined and sufficiently simplified, it can be meshed. Meshing consists of dividing the features of the geometric model into a set of finite elements. In this step the connections between the elements are also defined; From the obviously connected elements which are part of the same solid, to the more complex contact surfaces between assembly components. This section covers important concepts regarding meshing, and relates to Section 4.2, which covers more specific details for this thesis' meshing.

3.2.1 Element quality

Element quality is one of several metrics which attempt to identify poorly-shaped elements which invite calculation errors in a finite element analysis [14]. In ANSYS, the metric is a measure of how close an element is to its ideal shape: For a 2D quadrangle element, the element quality is 1 if it is entirely square, and decreases towards 0 as it deviates from this ideal. Other metrics may identify more specific ways in which the element deviates, while element quality remains rather general [3].

Mathematically ANSYS defines the element quality of an element as a function of volume V (for 3D) or area A (for 2D/shell) and edge lengths L_e :

$$Q_{3D} = C \frac{V}{\sqrt{(\sum L_e^2)^3}} \quad Q_{2D} = C \frac{A}{\sum L_e^2} \quad (1)$$

Where C is some constant which varies between element types (e.g. brick, pyramid, and wedge elements).

CAE Associates [10] performed a simple demonstration of poorly shaped elements skewing results, without going into much technical detail. For technical detail, Shewchuk [14] has a review of several 2D element quality metrics, and proposes a few of his own based on the calculable mathematical errors introduced by sub-optimal element shapes. Cook describes misshapen elements more qualitatively,

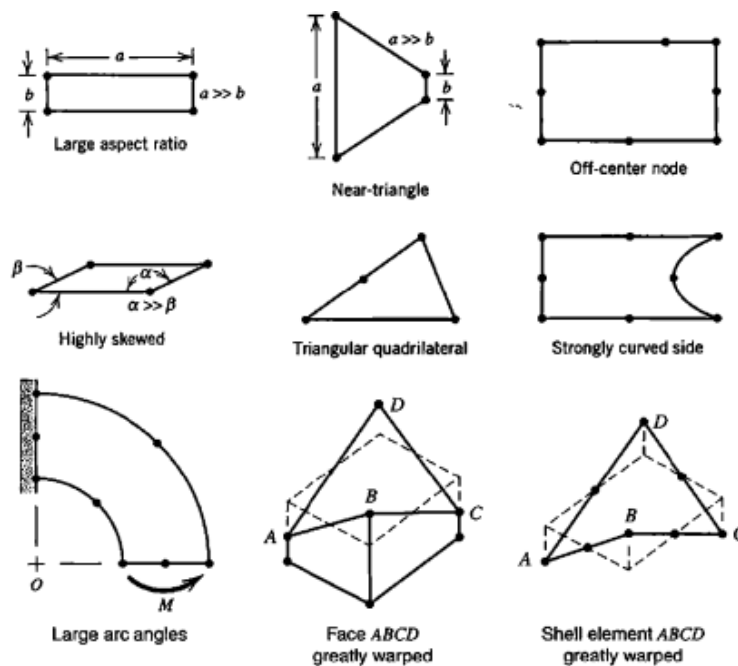


Figure 6: *Element shape distortions that may reduce accuracy [6].*

specifically correlating which errors surface from combinations of distortions in different element types [6, pp. 340–341]. Covering every such combination (and every metric which would detect them) would bloat this thesis; As shown in Figure 6, there are many ways an element can be misshapen, and many ways this can lead to inaccuracy. ANSYS supplies several more metrics, e.g. Jacobian ratio, skewness, aspect ratio, and warping factor, and it is good practice to monitor these values when working on large models where poor element quality might not be immediately obvious.

3.2.2 Element type

Elements come in many shapes, but even similarly shaped elements may have differences. Without touching on elements suited for different analyses (e.g. fluid and thermal), structural elements themselves differ in node amounts (e.g. mid-side and centre nodes), explicit or explicit integration, axisymmetry, and of course basic shape. The ANSYS user manual [3] features an exhaustive list of its featured

element types, two of which were used for this thesis' simulations.

One of the element types is a standard solid element, but the other is a shell element. These are formed when ANSYS meshes a surface body with a specified thickness and normal direction. Shell elements are used for thin bodies, and can be significantly more efficient than solid elements, which often need several elements through a thickness to accurately model thin-body mechanics. ANSYS' relatively new SHOLSH190 element attempts to bridge the gap between solid and shell elements, but unless there is a component with variable thickness that stretches the limits of shell element applicability, these are not strictly necessary [3].

There is also a distinction between linear and quadratic elements; This does not refer to their shape but rather to the order of the interpolation functions they use between nodes; Linear elements use first-order shape functions, while quadratic elements use a mid-side node to form a second-order function. Extra nodes and higher-order functions lead to more calculation time, but the increased accuracy can let the user achieve the same results with far fewer elements. Cook [6] goes into great detail on the formulation of linear and quadratic elements, but states that both types have merits when comparing computation time and accuracy. Both Cook and the ANSYS manual [3] do however warn against using the degraded (e.g. triangular and tetrahedral) versions of the linear elements, especially in critical areas of the model.

During modal simulations errors can arise because lower-order elements cannot accurately emulate some deformation modes and instead compensate with unrealistic modes. High-order elements are in the opposite situation, sometimes displaying

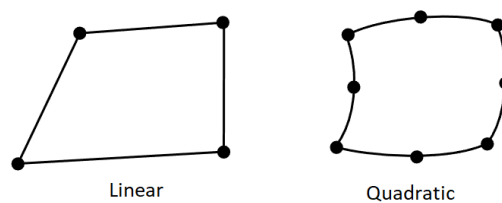


Figure 7: *Linear and quadratic 2D elements, comparable to SHELL181 and SHELL281 [3].*

deformation in unrealistic degrees of freedom. Cook again has a summary of different node types and the amount of spurious deformation modes they can present [6, p. 226]. Section 6.1.1 also shows a cursory comparison of results from both linear (SHELL181) and quadratic (SHELL281) shell elements.

3.2.3 Mesh refinement

ANSYS can create a mesh from a geometric model with just the push of a button, and a user might be satisfied with this default algorithm after tweaking some general sizing or refinement parameters. The suite offers some more advanced options, however.

Adaptive convergence uses e.g. stress gradients to identify areas of the mesh in need of refinement, performs automated refinement, and continues iterating over the simulations until values in this area converge [3]. The identification algorithm and refinement methods are described in the ANSYS manual [3] as well as by Cook [6, pp. 319–331]. Unfortunately, the technique was unavailable in this thesis' simulations due to interference by the ACP systems, which do not handle regenerating the mesh particularly well. The combined geometric model may also have been a factor in this.

Manually altering the mesh is also a core approach to mesh refinement. This ranges in directness from adjusting nodes by hand to lowering the global sizing parameter. In the mid-range lie the per-feature operations where one can e.g. specify the element sizing along one face or edge of a component. As described in Section 4.2.3, these were the most commonly used tools for this thesis. The tools allow the user to refine specific areas of the mesh where e.g. stress concentrations occur, and is usually more efficient than using adaptive convergence [3]. When meshing, ANSYS automatically recognises the smallest components of a model, and attempts to size elements accordingly [3]. For fine control, though, manual sizing options are extensive: Beyond the already mentioned edge, face, and body sizing options, one can also specify the size of select elements within a certain sphere or body of influence.

3.3 Materials

Each finite element of the model needs to know its own physical properties in order to assemble a proper stiffness matrix. For isotropic materials this is almost trivial; At the geometric modelling or meshing stage, whole components can be ascribed a material type with all necessary information, and every element of this material has the same properties. Section 4.3 summarises the isotropic materials used in this thesis. Composite materials are, however, more complex.

Before going deeper into the subject of composite material definitions, a brief summary of carbon fibre fundamentals may be in order. Carbon fibre parts consist of layers (laminae) of carbon fibres held together by a polymer matrix which keeps the fibres from simply buckling under compression or separating under non-axial loads. Carbon fibres can be arranged unidirectionally (parallel) within the matrix, or woven or stitched together (often perpendicularly, but other angles are sometimes desirable); The orientation of fibres determines the properties along different directions in the lamina. Laminae are stacked to form a laminate, which again combines the directional material properties of the laminae (Figure 10 visualises how properties vary by angle in such materials).

The above is a concise summary of an entire field of material mechanics. Entire works are dedicated to accurately calculating laminate material properties, although the ANSYS Composite PrepPost (ACP) system uses the more elementary classical laminate theory (CLT) [2]. This theory is called classical for a reason: It has been thoroughly documented in many previous works. Jones [12, p. 190] has a well-written and understandable section deriving the theory's equations, while eFunda [7] has a concise summary of the essentials. Jones' work also goes into detail on e.g. symmetric stack-ups of laminae, which is relevant for the plate stacks used in this thesis (see the last parts of Section 4.3.2).

Classical laminate theory requires the following information to calculate a laminate's properties:

- Lamina mechanical properties
- Lamina thicknesses

- Lamina orientations
- Stack-up order

In ANSYS Composite PrepPost, the above information can be supplied in three sections: Materials, fabrics, and stack-ups. “Materials” is the general material properties, often defined in the Workbench project interface before meshing; This includes densities, orthographic properties (e.g. stiffness in x and y direction), and so on. Defining a fabric simply means picking the fabric’s constitutive material and adding information of fabric thickness (as well as cost and more advanced draping options, if necessary). When a fabric has been defined, ACP can compute its polar properties, as shown in Figure 10. Stack-ups expand upon this by stacking multiple fabrics, given their orientation to each other in degrees. This allows it to define an entire laminate’s material properties, as shown in Figure 10.

Once the composite materials have been defined, they need to be applied to the actual elements of the structure. Again, this requires a sequence of information:

- The set of elements to apply composite materials to
- Laminate reference direction
- Stacking direction
- Composite material properties

Element sets must be defined earlier in the simulation workflow, e.g. during geometry definition or meshing; This simply involves defining a “Named Selection Set” in ANSYS. Each component should have its own selection set, unless they share laminate definitions, stacking direction, and principal laminate direction. This is because each selection set must be combined with a “Rosette”, which is essentially a coordinate system indicating the principal fibre direction of a laminate. Element sets are combined with rosettes to form “Oriented Selection Sets”—This is also when the user can specify the stacking direction. Oriented selection sets are finally turned into “Modelling Groups” by specifying the laminate material to be applied. One can also layer several stackups in a modelling group, for more complex layups.

To summarise: Element sets specify elements. Rosettes specify principal direc-

tions. Oriented selection sets combine the above with a stacking direction. Modelling groups combine this with the laminate definitions defined previously. Thus, each element finally has all the information it needs to form its own stiffness matrix, all of which are combined to simulate the entire structure.

3.4 Simulation setup

When a structure has a mesh of finite elements, one can perform a variety of simulations. To compare the structural performance of the airframe designs, this thesis uses modal and static structural simulations; Modal simulations give information of the structure's natural vibration modes, while static structural analyses help evaluate their performance under load.

Other simulations are possible, such as dynamic and harmonic response simulations. These can provide more detailed information of the structures, but require more information to set up, e.g. the frequency and magnitude of applied loads for a harmonic response simulation.

The following sections will contain some general information of modal and static simulation setup, while the specific simulation cases are described in Section 4.4 and 4.5.

3.4.1 Modal

A modal analysis is among the simplest analyses to set up, because modal frequencies are at their core a function of the structure's stiffness and mass distribution. This means that they are independent of loads, so lift forces and constraints do not need to be defined (unless one wanted modal frequencies when the drone was constrained, as constraints affect structure stiffness).

In addition to the airframe component masses, which are introduced to the simulation through material definitions, one also needs to define external masses like the propulsion system and batteries. This can be done at this stage of the workflow, but is more convenient to get out of the way during the geometry definition step, or during meshing, as changes at that point affect both static and modal analyses.

To prevent the simulation from running forever and finding enormous amounts of modal frequencies, ANSYS requires both a limited search range as well as a limited number of frequencies to find. The simulation runs until either the maximum number of frequencies is found, or all frequencies in the search band are found.

Modal frequencies are primarily functions of mass and stiffness, and the drones' payloads can be quite heavy. As such, some simulations were run as per Section 4.4 to estimate the extents of the payloads' effects on modal frequencies; Results are shown in Section 5.1.3. While there is a noticeable and sometimes drastic effect on certain modal frequencies, most modes are unaffected. Variable payload masses has variable effect on the frequencies as well, so unless one intends to perform a very specific analysis, it might be simplest to simply ignore the effects of payloads, or include the maximal expected payload to find the lowest possible frequencies.

3.4.2 Static structural

Unlike modal simulations, static structural analyses need to evaluate a static structure under some load. Applying just enough force at the propulsion mounts to make the drone hover does not constitute a "static structure", as any inaccuracy (which is unavoidable with FEM) would leave the system in disequilibrium. It is thus necessary to introduce a constraint somewhere on the drone without creating an unrealistic situation.

Generally, a static structural simulation of a drone is meant to simulate hovering. In this case, the drone is lifted by vertical force from its propulsion system and weighed down by its individual component masses as well as its payload. Gravity is simple to simulate when materials are properly defined, but the mass of the payload can also be treated as a fixed constraint to satisfy the static requirements. The simulations in this thesis uses this method, as is shown in Figure 11.

When using this approach, built-in tools allow the user to inspect the reaction forces in the fixed area. If all masses like avionics and screws are thoroughly included, the force should be equivalent to the weight of the payload, which can be a valuable method of verification: If the force is suddenly greater than expected, one may have for example set gravity in the wrong direction.

4 Numerical Model

As mentioned previously, the following sections will detail the simulation procedure in the order of the presented workflow. Consequently it will cover the particulars of the numerical model, from geometry and material definitions to meshing and the different simulation setups.

4.1 Geometry

This section describes the development process of the 3D models of both drones, and how these were simplified for simulations.

4.1.1 3D model development

Nordic Unmanned provided the original 3D models of both UAV designs, which were created in the Sketchup Pro software. They proved incompatible with the ANSYS simulation environment, however: ANSYS could not open the native Sketchup files, and the only file type that Sketchup could export that ANSYS could also open was STL. These files replaced curved surfaces with polygons, and lost information of components and their relations (i.e. all assembly geometry was considered one component). This could potentially make every following step of the workflow complicated and tedious. Similar problems occurred when attempting to import the ready-made model into other modelling software like Autodesk Inventor.

Fortunately the geometry was relatively simple, and needed to be simplified for simulation anyway. Thus it was reasonably efficient to create new, simplified models from scratch using Autodesk Inventor. Inventor's file types, IAM and IPT, are natively supported in ANSYS Workbench, but some errors surfaced when importing assemblies consisting of both solid and surface bodies. Using the STEP file format solved this issue, but removed some cross-updating functionality: After the STEP file was imported to ANSYS, it could no longer be edited in Inventor without needing a full re-import which reset progress.

As mentioned in Section 2.5, the two designs’ only differences were the plates, covers, and struts; Propulsion, batteries, booms, clamps, and legs were shared, and even the differentiating parts shared positional data. Thus, combining both designs in one file saved a considerable amount of time and effort. In this single 3D model file, the FX-8 and BG-200 components occupied the same space: When simulating, either set of differentiating parts could be suppressed (effectively removing it from the environment), leaving the “core” components as well as the parts specific for the opposite design.

This allowed for a more streamlined process in all succeeding steps, because actions like modifying battery mass distribution only had to be done on one model, and changes did not have to be synchronised between separate files and Workbench systems—Changes in the ACP system could be particularly tedious.

After importing the STEP file, the geometry was loaded into ANSYS’ own geometry software, DesignModeler, where key areas like propulsion mounts and battery footprints were imprinted onto the model. This allowed for easier definition of mass distributions, as well as forces in later steps.

4.1.2 Simplifications

In this project’s simulations, the entire propulsion system (motors, propellers, ESCs, mounts) was reduced to rudimentary masses distributed over the end of the booms. Batteries, similarly, were reduced to masses distributed over the “flaps” of the top plates (see Section 2.5). Payloads were incorporated as a fixed constraint in static simulations, and ignored in modal simulations apart from a specific study (see Sections 4.4 and 5.1.3). Avionic equipment was similarly ignored.

Numerous connections were simplified greatly: The aluminium clamps connecting the booms to the plates are machined to reduce weight, were modelled as simple, solid blocks here. The clamps connecting the landing legs to the booms were simply assumed rigid, making their geometry and material practically irrelevant. The material densities for both components were adjusted to match measured masses.

Bolted connections were systematically treated as bonded, ignoring any finer mechanics at play as well as their masses (though these were taken into account when weighing e.g. propulsion mounts and leg clamps). Bonded assumptions assume no slip between components, which runs the risk of introducing artificial stiffness; This can be detrimental to validity and became a minor issue during mesh refinement (see Section 6.1.2).

Newer versions of the drone also feature jointed booms which allow for more compact storage without disassembling the airframe. The joints are placed roughly midway along the booms, but for the purpose of this thesis they were entirely ignored.

Asymmetries in the design of the plates, mostly holes to route cables, were ignored because they varied between instances of the same design. Unfortunately this decision was made later in the process, after simulations were set up for full models. Simulations could potentially have been significantly more efficient if symmetry was assumed from the start; As an example, Bolek [4] experienced reductions in simulation times of 20 and 50 % for modal and structural analyses, respectively.

Apart from the initial plans of including asymmetric details, the ACP system was incompatible with symmetry without disruptive workarounds. Additionally, because the model was used for modal analyses, there was a risk of missing any anti-symmetric modes, as demonstrated by Skotny [15]. Results showed numerous antisymmetric modes, indicating that symmetry should be treated with caution.

4.2 Meshing

Once the simplified geometry was modelled, it was meshed as described in the following sections. The final mesh consisted of 206348 elements and 902040 nodes; Only quadratic elements were used, so there were 6 degrees of freedom per node. All component contacts were modelled as bonded, including contacts between covers and clamps which were strictly speaking frictional.

4.2.1 Element quality

After manually modifying the meshing methods (see Section 4.2.3), the average element quality as seen in Figure 8 rose to 0.95, with the lower-quality elements ($Q \approx 0.50$) confined to parts of clamps and covers which were of lesser importance. As the experiment by CAE Associates suggests, extremely high quality is not necessary for reasonable accuracy, but was in this case not difficult to achieve [10]. Figure 8 displays the element quality as a percentage of the entire model's volume, counting shell and solid volumes separately. As it makes quite clear, most of the volume is meshed by very high-quality elements while some solid elements make up the lower-quality ranges. Interestingly enough, there is a single shell element with a quality around 0.40. The results from this spot did not differ much from its symmetric equivalents around the plate, however.

4.2.2 Element types

Two element types formed the entirety of the mesh: SOLID186 and SHELL281. SOLID186 is a quadratic 3D brick element featuring 20 nodes: 8 corner nodes and 1 midside node for each of the 12 edges. When the meshing algorithm cannot fit a full hexahedron in the mesh, the element is degraded into a wedge (triangular prism), tetrahedron, or pyramid. SHELL281 is the "2D" equivalent, in that it only simulates the in-plane situation, then extrapolates the results over the shell element's thickness [6, p. 561]. This particular element sports 8 nodes (4 corners and 4 edges) and forms wedges when necessary. All nodes in both elements have six degrees of freedom: Rotation and translation in three dimensions [3].

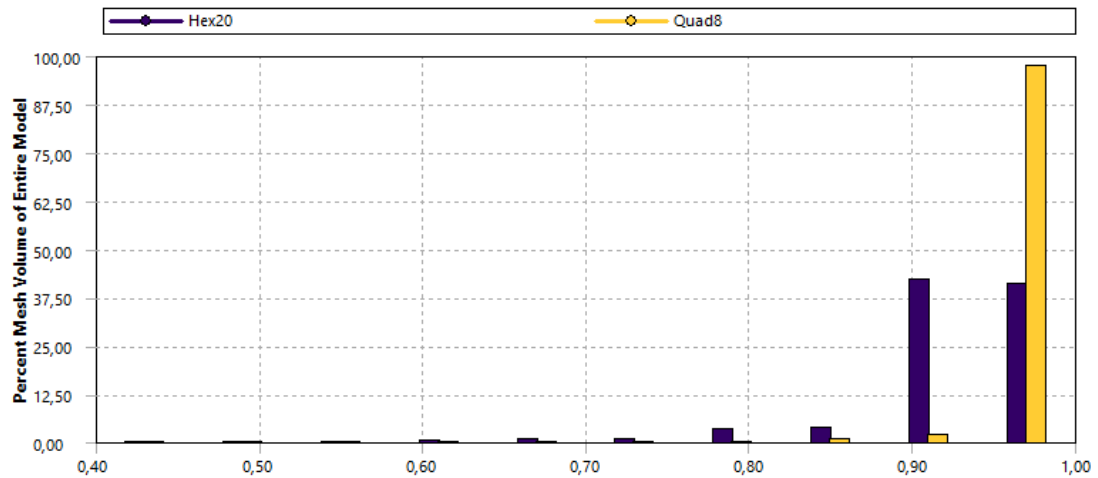


Figure 8: *Element quality as percent of entire model volume. Hex20 and Quad8 correspond to SOLID186 and SHELL281 element types respectively.*

4.2.3 Mesh refinement

Almost all components were meshed with a series of MultiZone method controls, which essentially splits models into more easily meshable parts, then combines these to form a cohesive mesh of the whole component [3]. Because the mesh was used for both modal and static simulations, it was kept mostly uniform by applying sizing commands to entire components or faces: If element numbers grew too high due to high levels of local refinement, modal simulation times exploded.

MultiZone method controls also allow the user to specify whether or not triangular/tetrahedral elements are allowed; This was generally set to force full hexahedral (hexa) or quadrangular (quad) elements. As mentioned, SHELL181 elements still formed triangles in the plates because they could not represent the many curved surfaces of the models accurately. SHELL281 elements, however, achieved this thanks to their quadratic side shapes [3].

Section 6.1.2 discusses the effect of mesh refinement on the results. Of the element sizes investigated, the final mesh used plate element size of 2.5 mm and boom element size of 7 mm.

4.3 Materials

This section will primarily focus on the composite materials of the airframes, as these comprised the majority of the structures. Isotropic materials were mostly limited to smaller, minor components.

4.3.1 Isotropic materials

Of all components on the drone, only a few were considered isotropic: Clamps, covers, struts, and leg clamps (which were considered rigid, so only density mattered). Both covers and struts were 3D printed, so assuming isotropy is a considerable simplification, but these components were not considered crucial for the analysis or for the structure as a whole. The clamp aluminium density was modified from ANSYS' default structural aluminium definitions to make the total mass of the simplified model match the actual measured mass of the components, as was leg clamp density.

Table 2: *Isotropic materials used in the simulations.*

Component	Mass [g]	Material	Density [kg/m^3]
Clamps	7	Aluminium	1141.7
Covers	10	FDM Nylon 12 [8]	724.3
Struts	1	FDM Nylon 12 [8]	724.3
Leg clamps	64	Rigid	867.2

4.3.2 Composite materials

The carbon fibre, or fibre-reinforced polymer (FRP) components are more complicated. Nordic Unmanned has used different carbon fibre suppliers over time, each using different techniques and layups with sparse documentation. As such, the composite materials simulated in this thesis are generalised from publicly available information supplied by EasyComposites, a British FRP supplier.

Composite material parts were assumed similar to EasyComposites' products, namely their quasi-isotropic "High Strength Carbon Fibre Sheet" [11] and "30 mm (27 mm) Woven Finish Carbon Fibre Tube" [1]. Available specifications for both products include their laminate definitions as well as fibre properties: Fibres are mainly sourced from Pyrofil [16], except for some layers of Zoltek fibres in the plates [18].

Fibres are only half of the FRP mix, but EasyComposites does not go into detail on matrix properties apart from calling the plate matrix high-performance epoxy and stating that the tube material is pre-impregnated (prepreg). The exact type of resin is not of great significance, however, especially since the other material properties are generalised; Resin types have been shown to have relatively low influence on laminate properties [13].

All fibres used in the above components have elastic moduli of roughly 230 GPa: The Pyrofil 3k fibres (3k meaning that the fibre consists of 3 000 filaments) have a modulus of 234 GPa, the 12k and 15k both land around 240 GPa [16], and the Zoltek lamina modulus is 242 GPa [18]. One cannot simply put these values into material definitions, as the lamina properties are affected by the volume fraction of polymer to fibres as well as weave method (if applicable) [9] [13].

The U.S. Department of Defence has a handbook filled with laminate material properties [5], and while it may have proven useful for extrapolating material properties from the previously mentioned fibres, ANSYS' built-in material library proved itself sufficient; Perhaps not coincidentally, the library comes with standard properties for woven and unidirectional composite materials of carbon fibres with moduli of either 230 GPa or 395 GPa, with variations depending on resin and manufacturing type.

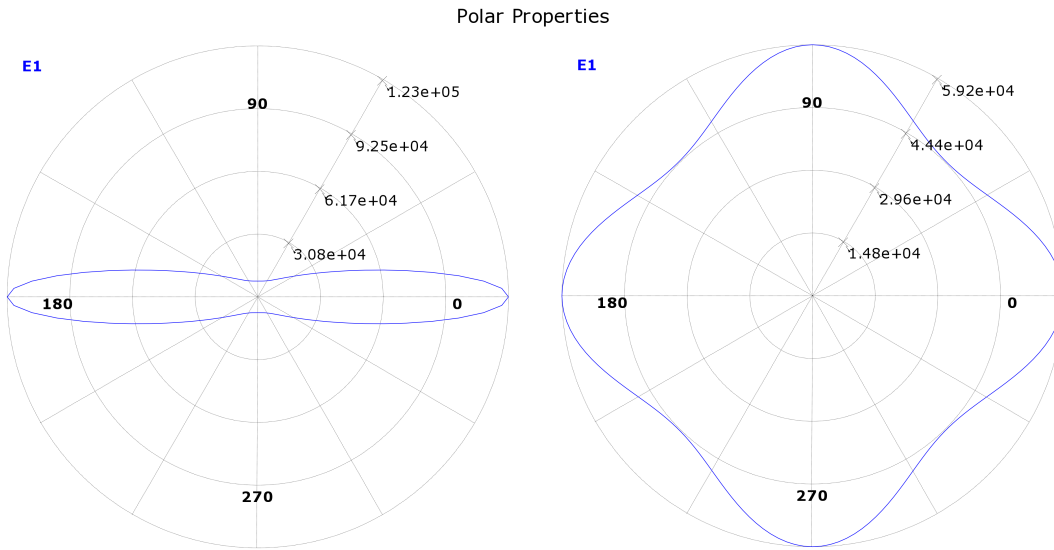


Figure 9: *Polar elastic modulus (MPa) of two fabrics used in this thesis. Left: Unidirectional Pyrofil 200 gsm. Right: Woven Pyrofil 650 gsm.*

Table 3: *Lamina properties for wet 230 GPa modulus carbon fibre laminae, woven and unidirectional (UD): Young's moduli (E), Poisson's ratios (ν), and shear moduli (G).*

Fibre type	E [MPa]			ν			G [MPa]		
	X	Y	Z	XY	YZ	XZ	XY	YZ	XZ
Woven	59160	59160	7500	0.04	0.3	0.3	17500	2700	2700
UD	123340	7780	7780	0.27	0.42	0.27	5000	3080	5000

Because all the fibres listed above fell near 230 GPa, these presets fit well with only minor edits to density due to some heavier fibres, as well as further adjustments to fit densities to the measured masses of the various components. Wet variations of the composites were also used: Their default densities matched the measurements better than the prepreg versions, and they made for a more conservative estimate stiffness-wise. The lamina properties are listed in Table 3, while the fabrics used are listed in Table 4.

Table 4: *Fabric definitions. Note: “gsm” (g/m^2) designations from the EasyComposite catalogue are invalid due to density adjustments.*

Fabric	Type	Thickness [mm]	Material	Density [$10^{12}kg/m^3$]
Pyrofil 200 gsm	Woven	0.25	TR30S 3k	1.79
Pyrofil 250 gsm	UD	0.20845	TR50S 15k	1.6
Pyrofil 650 gsm	Woven	0.65	TR50S 12k	1.82
Zoltek 300 gsm	UD	0.175	PX35	1.81

Table 5: *Composite stack-up definitions for tubes (booms and legs) and plates. Subscripts indicate repetition of a stacking sequence. Thickness is for the entire laminate.*

Component	Fabric	Angles [°]	Thickness
Tubes	Pyrofil 200 gsm	0	1.5 mm
	Pyrofil 250 gsm	[90, 0] ₃	
Plates	Pyrofil 200 gsm	0	2.5 mm
	Zoltek 300 gsm	[45, -45]	
	Pyrofil 600 gsm	0	
Even symmetry			

From the fabrics, the stackups were defined primarily through EasyComposites’ own descriptions of the component layups. The tubes consist of alternating layers of unidirectional Pyrofil 250 gsm fabric, topped with a woven finish, reaching a final thickness of 1.5 mm. Meanwhile, the company doesn’t actually deliver the 2.5 mm plates featured in both airframe designs, only 2 and 3 mm (± 0.3 mm). Both of these have defined stack-ups, however, which were be adapted to a 2.5 mm version. Table 5 lists the laminate stack-ups, while polar properties are shown in Figure 10.

The laminate used in the tubes displays an expected amount of anisotropy, considering how it is mostly formed from perpendicular unidirectional laminae. Meanwhile, the plates appear (almost) entirely isotropic in the plane. This is known as quasi-isotropy, because the laminate appears isotropic in one plane although it consists of anisotropic layers, and is still not isotropic in thickness direction. Jones

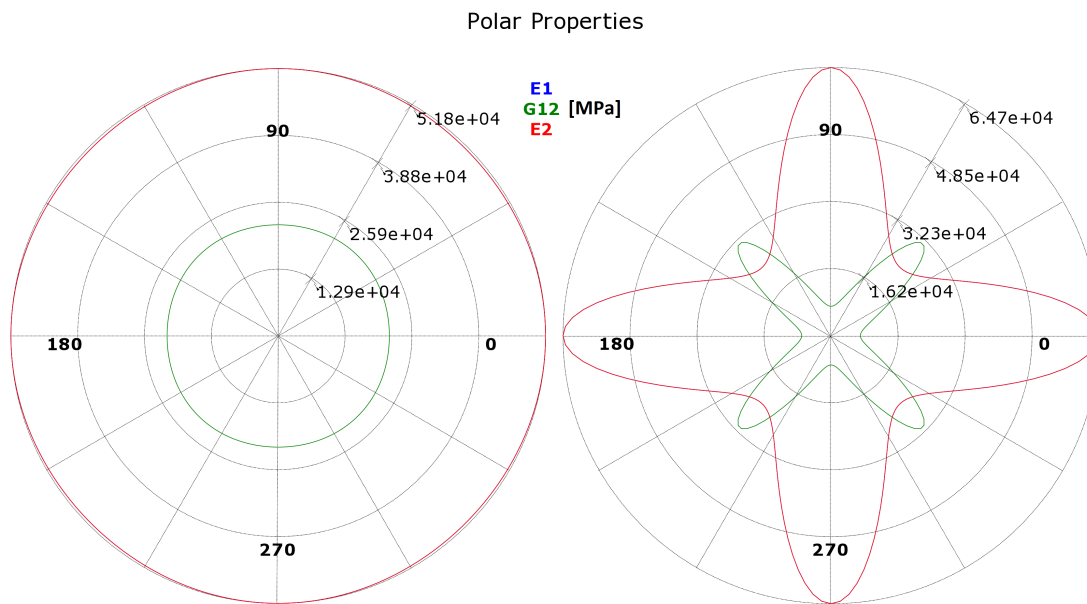


Figure 10: *Polar properties of this project's two composite stack-ups. Left: Plates. Right: Tubes (booms and legs).*

[12, p. 219] has covered the mechanics of this, but it should be noted that this laminate achieves quasi-isotropy without all lamina being of the same thickness, nor even the same type (as it mixes both unidirectional and woven laminae).

Overall, the laminate properties appear within expected ranges. Because the analysis of the two airframe designs was relative, discrepancies and inaccuracies in material definitions are not expected to have an overwhelming impact on validity. For an absolute quantitative analysis, however, one might desire more thorough documentation of material definitions.

4.4 Modal analysis

Information on propeller and motor models (provided by Nordic Unmanned) combined with from data tables supplied by the manufacturer, gave an impression of the operating range of the drone. Table 6 lists the rotational speed of the propellers in RPM and Hertz at different throttle levels. Nordic Unmanned expressed that each motor's throttle is usually kept between 40 % and 60 %.

Very little input was needed to set up the modal analyses once the meshing and material definitions were complete. Simulations were configured to find frequencies between 0 and 500 Hz to cover the range of motor rotation frequencies, though ideally the limits would be based off measured vibration frequencies from the motor.

Modal frequencies are functions of mass and stiffness, so naturally the drone's payload was suspected to be a considerable factor. To investigate the effect, payloads of 2.5 kg and 8 kg (corresponding to a moderate and large payload) were added to the FX-8 modal simulation case; The mass was applied to the bottom plate's centre at a diameter of 140 mm (see Figure 11). Simulations only ran up to the first 40 modes, to cut down on simulation time. Because the results emerged quite early in the process, their results (listed in Section 5.1.3) prompted the choice of dropping payloads from all other modal simulations.

Table 6: *Propeller RPM at different motor throttles.*

Throttle	RPM	Hz
40 %	1896	199
50 %	2268	238
60 %	2581	271
100 %	3709	388

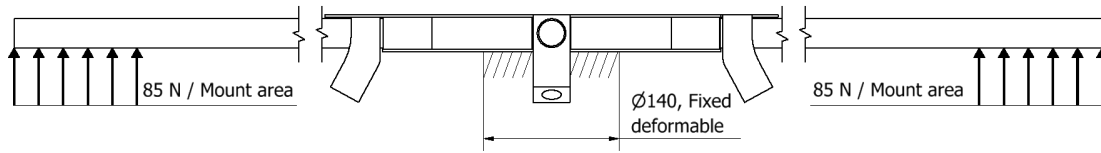


Figure 11: *Static load case. Landing gear and out-of-plane booms are not displayed. Fixed support applied at centre of bottom plate, as a deformable body-to-ground joint. Gravity was simulated for all parts, including propulsion and batteries.*

4.5 Static structural analysis

The static structural load case aimed to emulate the drone hovering while loaded beyond maximal payload capacity. By design, the maximum take-off weight is 25 kg; A factor of 1.4 was applied to simulate an extraordinarily high load, putting a force of 85 N on each boom—although this is still technically within the biaxial propulsion system’s capabilities. Figure 11 shows a schematic of the load case.

In practice the different payloads are fastened to the airframe in different ways, but in these simulations the connection was emulated as a deformable fixed joint between the bottom plate and “ground” (alternatively a payload just heavy enough to make the drone hover). The joint was given a limited sphere of influence, affecting elements within 70 cm of the plate centre.

ANSYS calculates reaction forces at supports and joints, so this method can also be used for validation: The moments and horizontal forces at the joint should be practically zero, while the vertical force should equal the weight of payload, avionics, and any other masses not directly included in the model.

Though the load case may not be the absolute maximal stress applied to the structure (compared to dynamic loads from acceleration or accidents), it is expected to be a suitable environment to investigate the relative strength of each design; Establishing the exact failure criteria was not the goal, and would be fraught with errors especially due to the uncertain material information (see Section 4.3).

5 Results

This section will present the results of all simulations in brief. There will be some initial interpretation of the more qualitative data, especially modal frequency distributions, though the bulk of discussion is contained in Section 6. Modal analysis results are presented first, covering modal frequencies, modal shapes, and the effect of payloads. Finally static structural results are presented, including the numerical results and charts of stress distributions in the airframe plates.

Simulations for were run in ANSYS Workbench Release 17.0, on the Windows 10 Education x64 operating system, running on a 6-core CPU at 3.6 GHz. ANSYS had 64 GB RAM available to it; Most simulations used up to 60 GB, and simulation times drastically increased when this was exceeded; When ANSYS cannot access enough high-speed RAM to store its calculations, it can instead write the data to disk, which can reduce speed by a factor of 10 [3].

Table 7: *Solution times in processor seconds for different simulations.*

	FX-8	BG-200
Modal	653	1210
Static	325	456

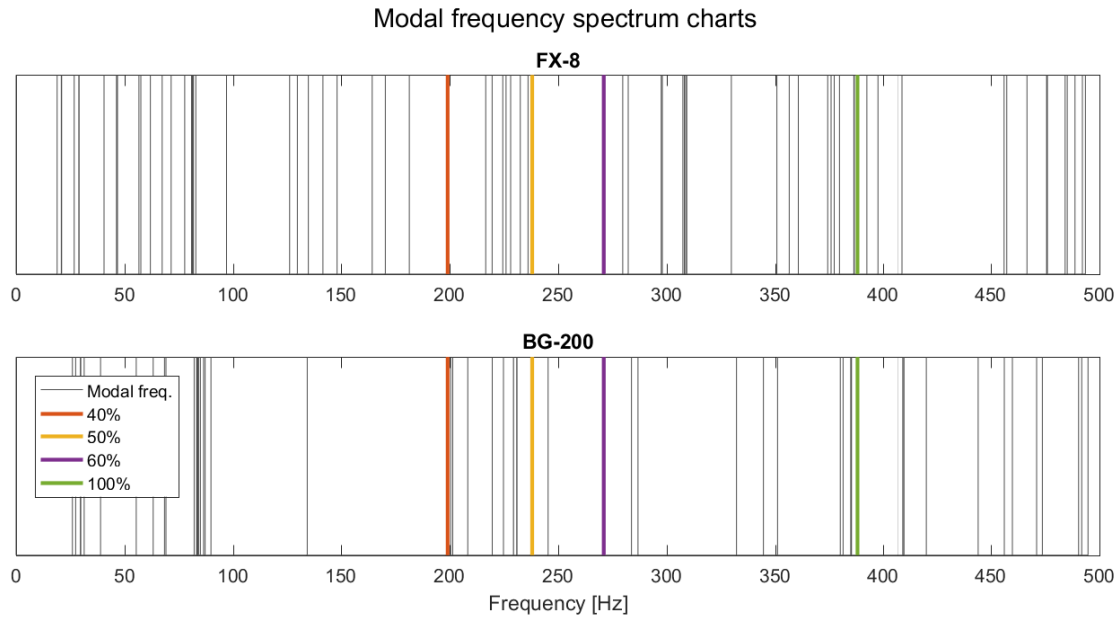


Figure 12: *Modal frequency spectra, highlighting frequency spread and ranges free of modal frequencies. Key throttle values marked in colour.*

5.1 Modal analysis

The primary outputs of a modal analysis are the modal frequencies and their corresponding shapes. This section presents the frequencies and their distributions within the operating range, discusses some common features of the modal shapes before grouping them, and finishes with a short study on the effects of payload on the modal frequencies.

5.1.1 Modal frequencies

Simulations of the BG-200 and FX-8 designs respectively returned 60 and 73 modal frequencies in the range of 0 to 500 Hz. ANSYS presents these results similarly to Figure 13 (albeit without throttle values). A representation like Figure 12 highlights the range of frequencies in higher fidelity, but does not communicate the number of modes as clearly. Note that the plot of the BG-200 frequencies in Figure 13 has been padded to balance the graphs: These modes above 500 Hz were

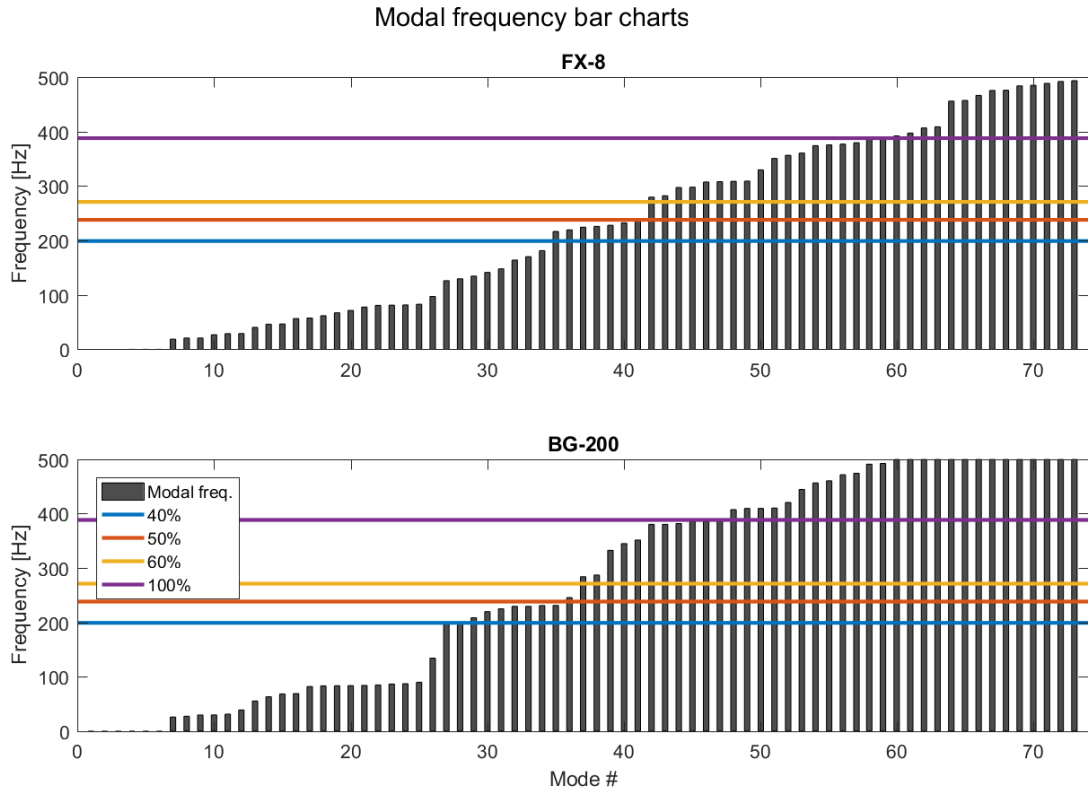


Figure 13: *Modal frequency bar chart, as favoured by ANSYS. Key throttle values marked in colour.*

not actually simulated.

At the low frequencies between take-off and operating frequencies, both designs pass through several resonance frequencies, but the modes of the FX-8 design appear far more evenly distributed than those of the BG-200; In that design, a large amount of modes (modes 17–25) lie tightly clustered in the 80–90 Hz range. Most of these modes (see Section 5.1.2) feature prominent deflection of the landing gear legs, combined with various deformations of the core plates. Do note that mode shapes and numbers do not necessarily match between the two designs, as seen in Figure 14.

Between 40 and 50 percent of full throttle, the FX-8 design is the one with more closely packed modal frequencies. This does leave a gap near 40 % throttle, how-

ever. At this stage mode shapes are often combinations of lower-frequency shapes, but one noticeable trend is the torsion in the booms. Realistically modelling the rotors' gyroscopic effect would probably affect these frequencies, as might more accurately modelling the motor mounts fastened at the end of the booms.

Both designs appear to have a sweet spot between 50 and 60 % throttle, entirely (or at least nearly) free of modal frequencies. The BG-200 model also has large clear ranges between 60 and 100 %, but the drones are usually not used at this level.

Generally, the BG-200 model has fewer modal frequencies in its operating range, almost certainly due to the increased stiffness from the centre plates raising many frequencies out of the relevant spectrum. The redesign has also affected the distribution of frequencies, most notably gathering the lower frequencies based on landing gear vibrations.

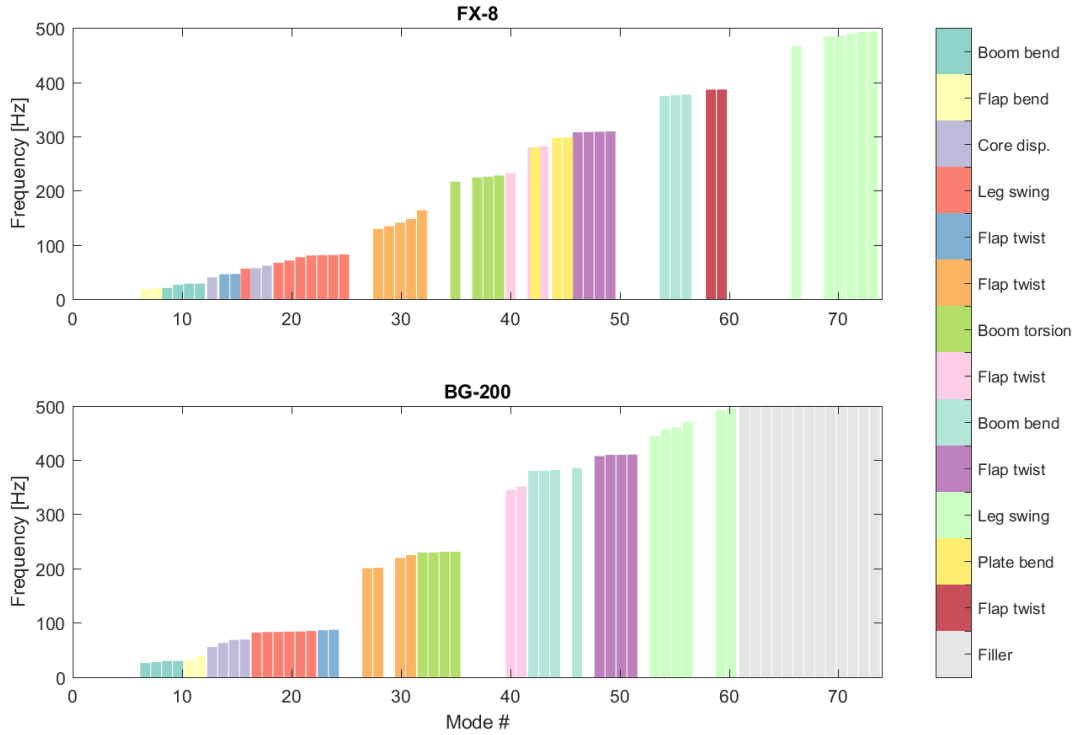
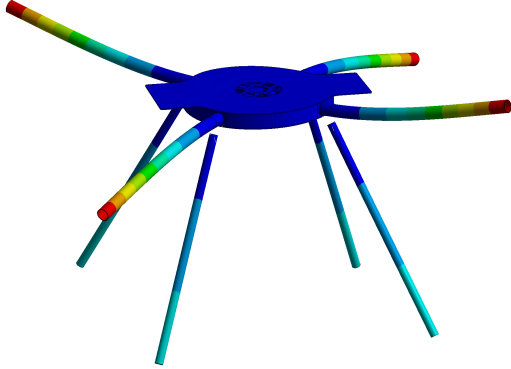
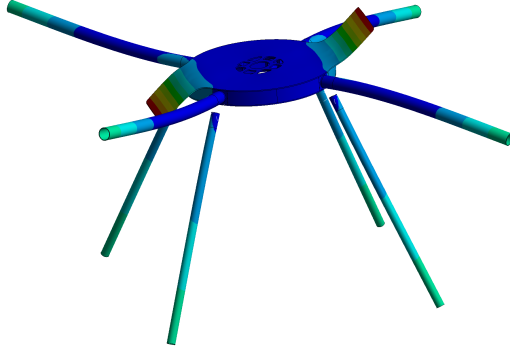
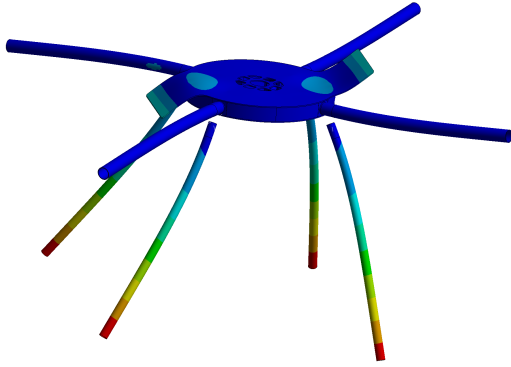
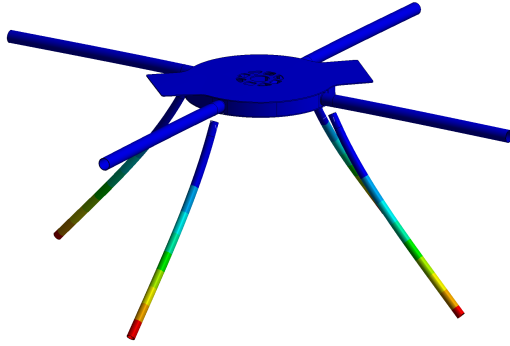


Figure 14: *Distribution of mode shapes over frequency. Modes combining several shapes are omitted. Shape categories are ordered as in Table 8.*

5.1.2 Modal shapes

Among the many modal shapes identified by the simulations, most display similarities to each other; Some appear to be combinations or variations of other shapes, drastically reducing the number of truly unique shapes. Table 8 shows a broad categorisation of modal shapes from the simulations, omitting combinatory shapes. While the descriptions of some shapes are identical, the groups usually vary in complexity between iterations. Figure 14 indicates where the different modes appear on the standard modal frequency chart. Note however that modes not demonstrating a distinct shape (i.e. combinations of other shapes) are omitted. For a full overview of the modes and their positions in the frequency spectrum, see Section 5.1.1 and Figures 12 and 13.

Table 8: *Common mode shapes and the modes which primarily exhibit them.*

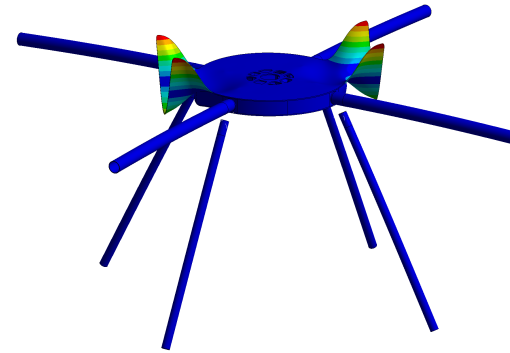
Mode image	Mode numbers		Mode image	Mode numbers	
Mode description	FX-8	BG-200	Mode description	FX-8	BG-200
	9–12	7–10		7, 8	11–13
Bending of booms			Bending of battery flaps		
	13, 17, 18	13–16		16, 19–25	17–22
Core rotation			Bending of legs		

Continuation of Table 8

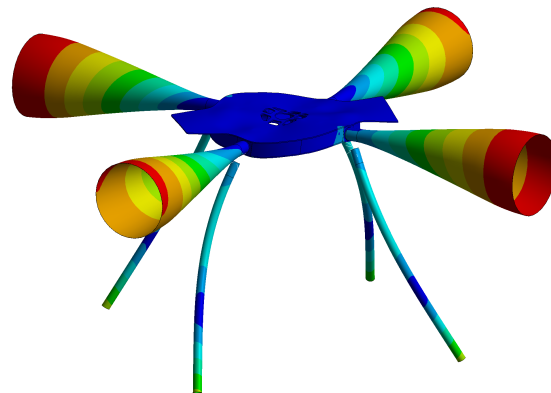
Mode image	Mode numbers		Mode shape	Mode numbers	
Mode description	FX-8	BG-200		FX-8	BG-200



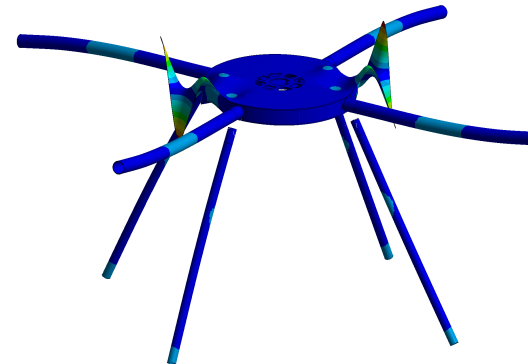
Twisting of battery flaps 14, 15 23, 24



Twisting of battery flaps 28–32 27–31



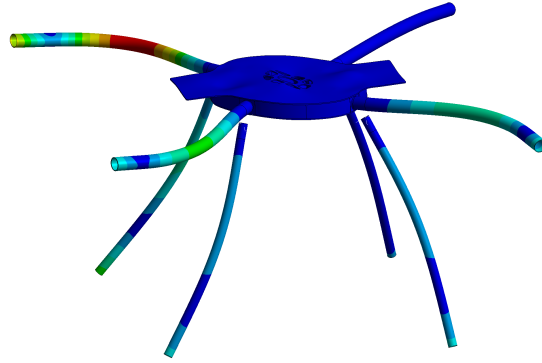
Torsion of booms 35, 37–39 32–35



Twisting of battery flaps 40, 43 40, 41

Continuation of Table 8

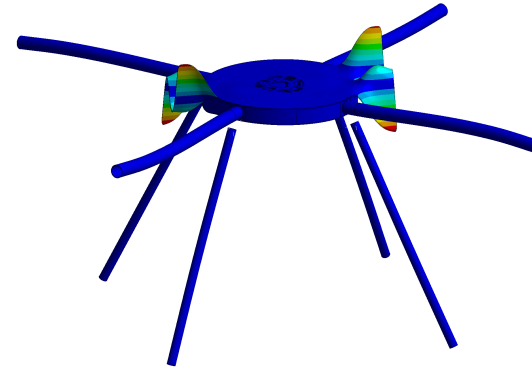
Mode image	Mode numbers		Mode shape	Mode numbers	
Mode description	FX-8	BG-200		FX-8	BG-200



Bending of booms

54–56

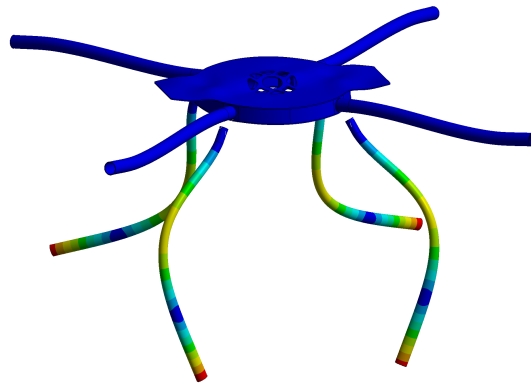
42–46



Twisting of battery flaps

46–49

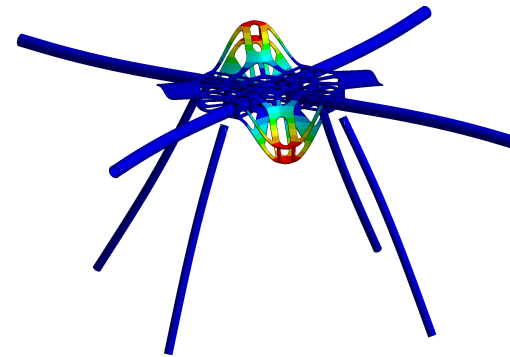
48–51



Bending of legs

66, 69–73

53–60

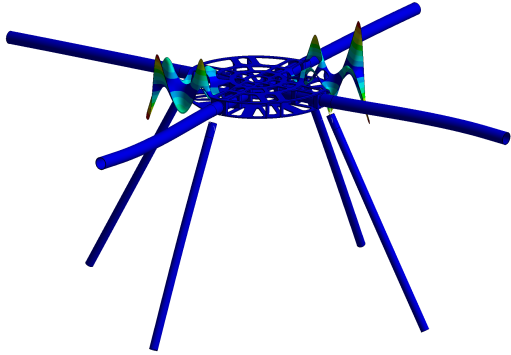
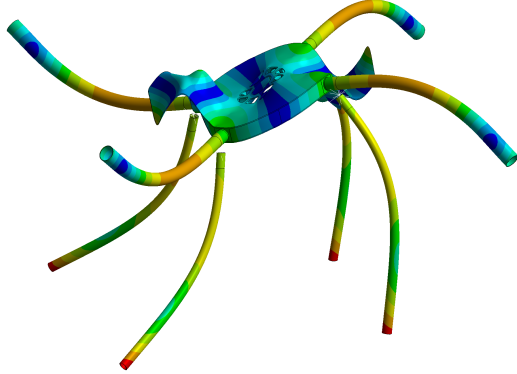


Bending of plate

42, 44, 45

N/A

Continuation of Table 8

Mode image	Mode numbers		Mode shape	Mode numbers	
Mode description	FX-8	BG-200		FX-8	BG-200
	58, 59	N/A		Various	
Twisting of battery flaps	58, 59	N/A	Combinations	Various	

5.1.3 Effect of payloads

To conserve simulation resources, the payload simulations were only run on the FX-8 model and its lowest 40 modal frequencies. Results are presented in Figure 15. Relative difference d_{rel} is calculated from frequency without payload f_0 and with payload f_{pl} :

$$d_{rel} = \frac{f_0 - f_{pl}}{f_0} = 1 - \frac{f_{pl}}{f_0} \quad (2)$$

The introduction of payloads has a noticeable effect on certain modal frequencies: One of the lowest frequencies decreases by 30 % with a large payload. Predictably, the most affected modes feature large movements of the drone's core, which is where the payloads are fastened. In a way the plots of Figure 15 can be used to identify modes with core movement, with whatever utility this might bring. For most modes, however, the effect appears to be quite limited.

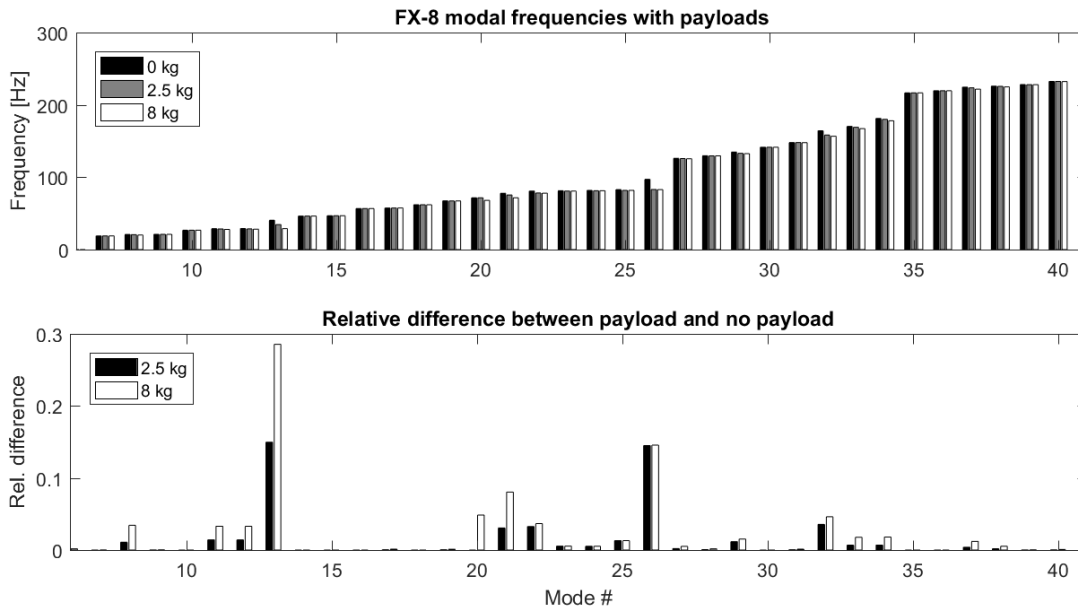


Figure 15: *Effect of payload mass on modal frequencies in the FX-8 design.*

5.2 Static structural analysis

This thesis is primarily a comparative study of the two airframe designs and not an in-depth analysis of specific strength of each design. Thus the post-processing tools in the ACP package were not strictly necessary; The many failure modes and criteria of FRP materials were not considered, only the relative performance of the two designs. Equivalent von Mises stress was used as a basis for the comparison, as was the total deflection of the booms.

Table 9 summarises the simulation results. Again, the relative values are of greatest import, and give some interesting information: The BG-200 model reduces total boom deflection by 19 % with its more solid plates. Stresses in the booms increase as well, although the 10 % increase might be grounded in model inaccuracy.

Figure 16 shows the stress distributions over the plates.

Table 9: *Deflection and maximal stress in airframe components.*

	FX-8	BG-200	BG/FX
Boom deflection [mm]	4.06	3.29	0.81
Boom stress [MPa]	90.5	101.3	1.12
Top plate stress [MPa]	58.8	24.6	0.76
Bot. plate stress [MPa]	42.9	32.5	0.42

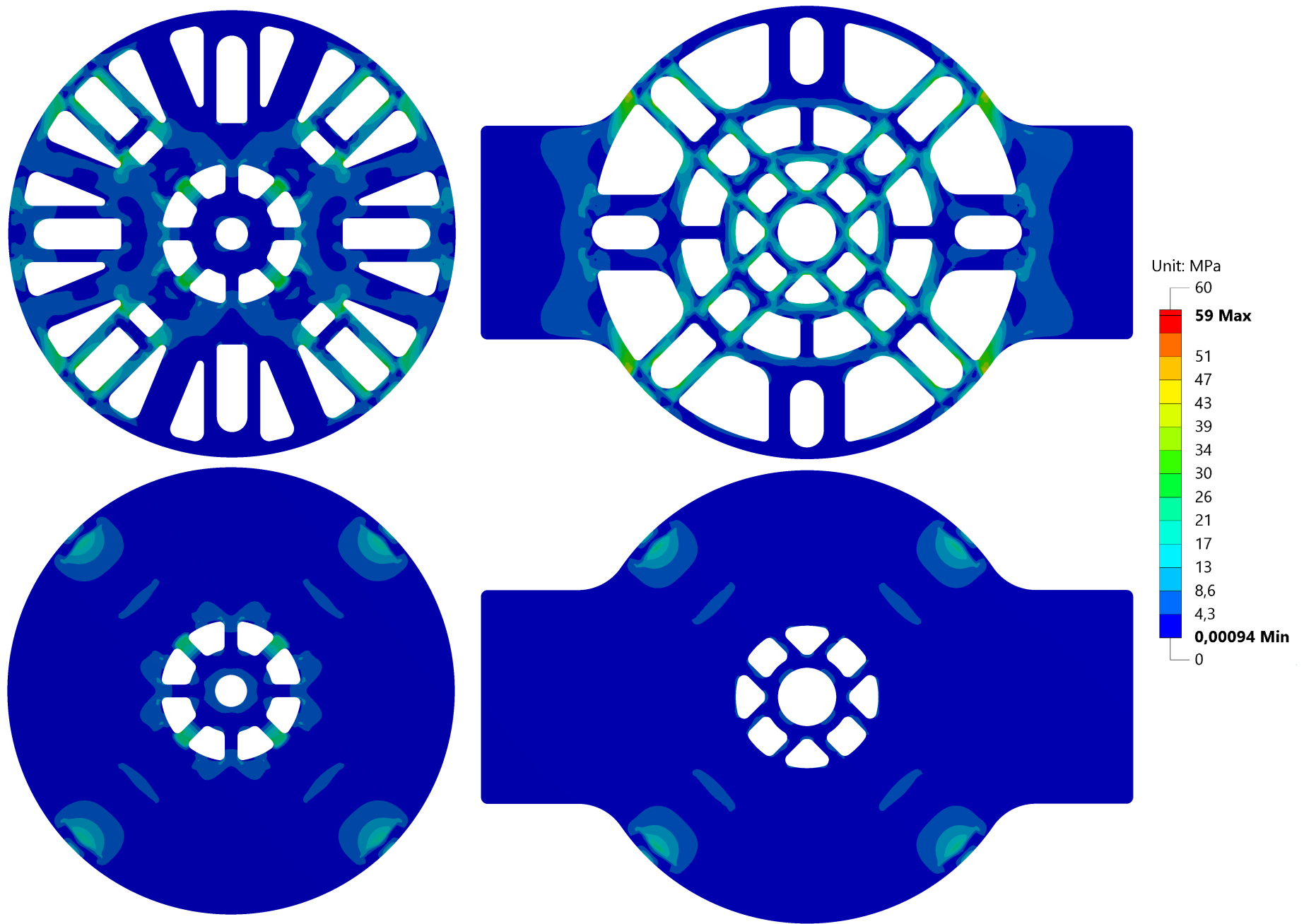


Figure 16: *Plate stress distributions shown by equal scale (MPa). Top plates are seen from below, bottom plates seen from the top.*

6 Discussion and conclusions

Before Section 6.2 discusses the implications of the presented results, their validity and caveats are considered in Section 6.1. While that section also indicates possibilities to improve validity, Section 6.3 specifically details prospects for future work.

6.1 Validity

Several simplifications and assumptions were made over the course of the project. Section 4.1.2 lists the key geometric simplifications, while the description of materials in Section 4.3 mentions simplifications and assumptions related to materials. Sections 4.4 and 4.5 also describe how the drones' states were reduced to simple calculable problems.

For future studies, the trustworthiness of the results could be increased in several ways, related to the previously mentioned sections:

- Simulating bolts, screws, and other miscellaneous components of the airframe
- Including the avionics masses and their distribution
- Including smaller details in the plates
- Fully modelling leg clamps

Using symmetric simulations may conflict with some of the above, and should be used with care when performing modal analysis, but could also reduce simulation time considerably.

Deepening the knowledge of the composite materials used would improve the accuracy of simulations, especially because the FRP components play major roles in all simulations. If one only aims to investigate modal frequencies and harmonic response (and not accurately simulate materials), experimentally determining stiffnesses on a component-grade level can give satisfactory results as well while reducing complexity significantly [17].

6.1.1 Effect of element type

As mentioned in Section 4.2.2, simulations were run with SHELL181 elements before switching over to SHELL281 elements. Some changes were made to the mesh after the switch, most notably a slight increase to plate element size to stay within computer memory limitations. This allowed for a coarse comparison results for the two element types. Figure 17 shows the relative difference d_{rel} in modal frequency value between the two simulations, calculated as:

$$d_{rel} = \frac{f_{281} - f_{181}}{f_{281}} = 1 - \frac{f_{181}}{f_{281}} \quad (3)$$

where f_{X81} is a modal frequency found using the SHELLX81 element, X being 1 or 2.

The results indicate that the SHELL181 elements generally report lower frequencies, varying noticeably by mode: Some modes are reported to have practically identical frequency, while some reach a difference of 15%. In the ranges of highest discrepancy, modes display torsion of the booms as well as prominent bending of plates and booms. Interestingly, the prominent ranges of almost equal results in the FX-8 simulations correspond to modal frequencies which almost exclusively feature different kinds of plate deformation. In general, the highest difference appears to occur in modes where tubes are subject to bending or torsion, which agrees with common convention that linear elements are ill-suited for such situations [6]. Table 10 also supports conventional wisdom, in that the maximum deformation, which in all simulations is the deflection of the booms, is simulated to reasonable accuracy. Stresses, however, display significant differences.

This difference in results might not have much impact on a study like this thesis, where relative performance of two designs is paramount. Although the difference in results varies between the FX-8 and BG-200 simulations, the error introduced is less fatal when considering relative values. That said, this case exemplifies how element choice can drastically affect the validity of results.

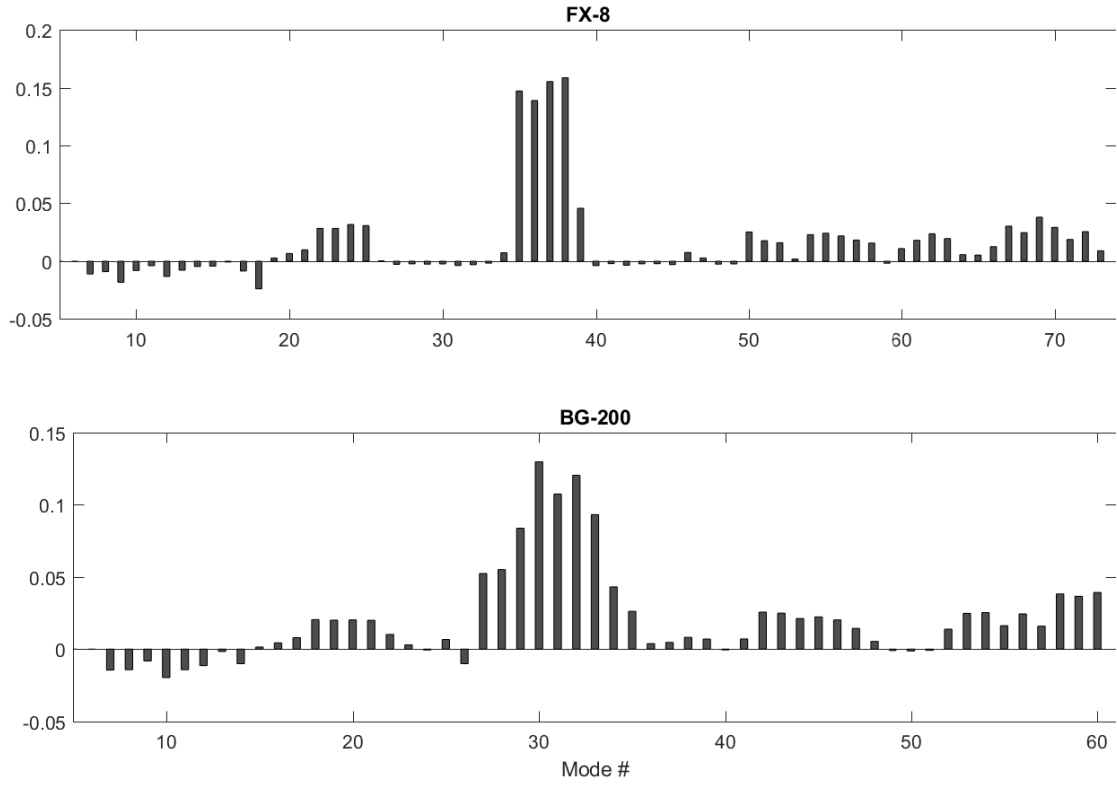


Figure 17: *Relative difference in modal frequency value between SHELL181 and SHELL281 elements.*

Table 10: *Relative difference in static simulation results between SHELL281 and SHELL181 elements.*

Measurement	Relative difference [%]	
	FX-8	BG-200
Max. deformation	1.56	1.56
Max. stress	22.7	31.0
Max. stress top plate	32.7	22.7
Max. stress bot. plate	9.20	8.20

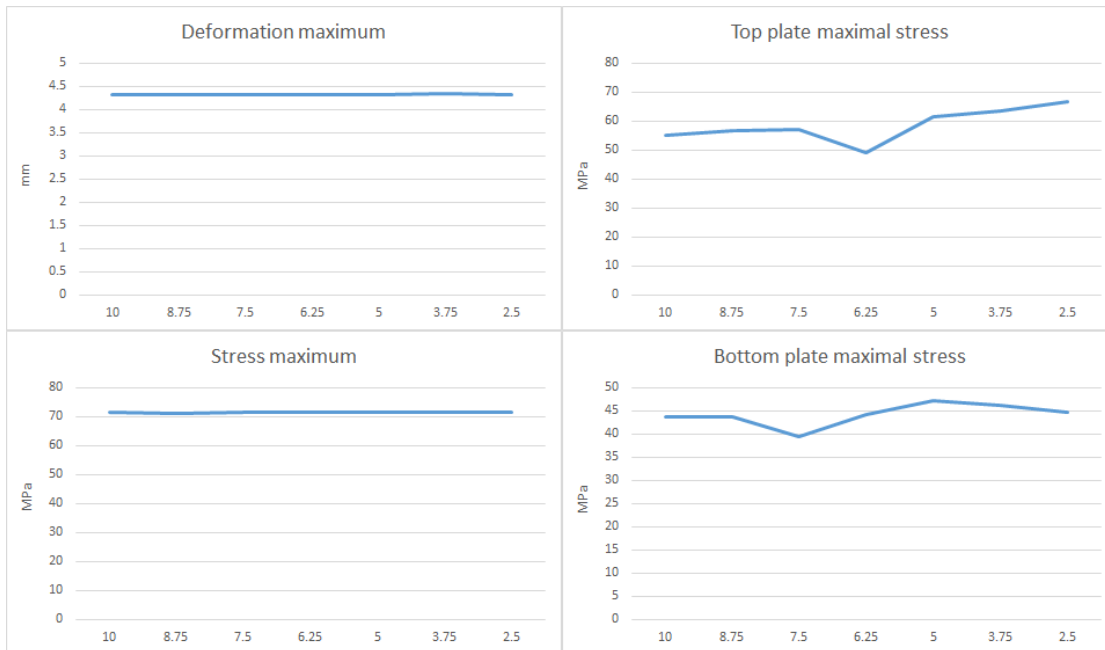


Figure 18: *Effect of plate element size (mm) on results.*

6.1.2 Effect of element size

Element size can drastically affect results in many ways, most notably near stress concentrations. While a relative study such as this is not as dependent on exact results near such concentrations, it is still desirable to have a mesh which can at least capture concentrations with reasonable accuracy. Unfortunately, ANSYS' adaptive convergence was not compatible with either ACP or the unified geometric model used in this thesis. Thus the mesh study was performed manually, and consequently has a limited amount of data points. To conserve simulation resources, the mesh was investigated on the FX-8 model using static structural analyses as described in Section 4.5.

Figures 18 and 18 show the progress of results as element size decreases for plates and booms. While one component's element sizes were changed, the others' remained constant.

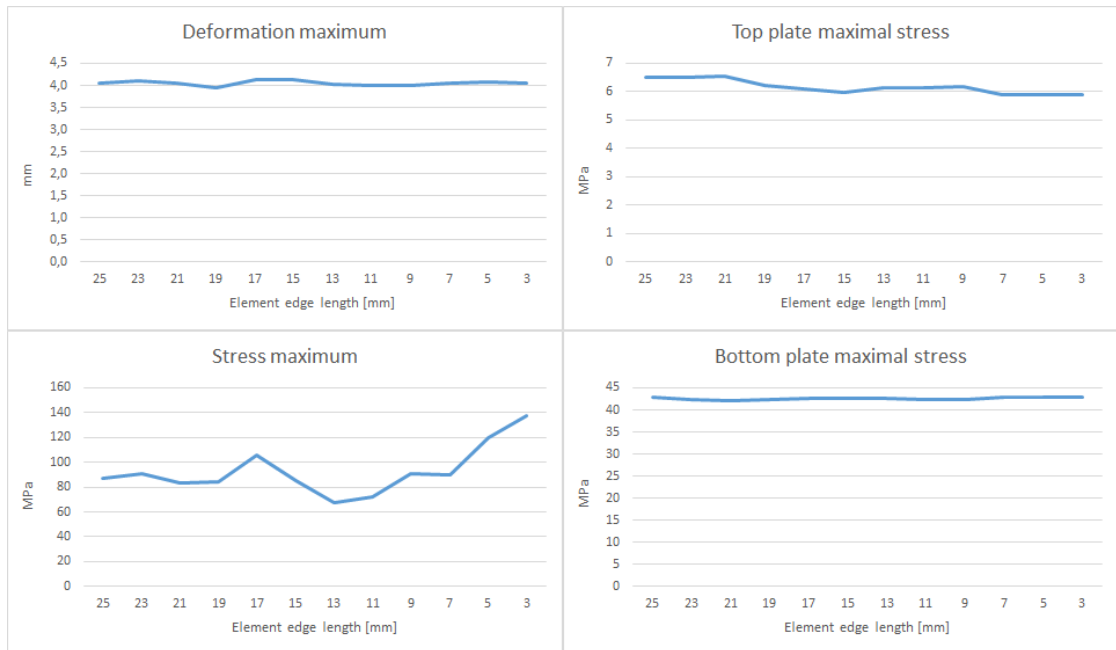


Figure 19: *Effect of boom element size (mm) on results.*

Plate element size appears to have little effect on the boom deformation or stresses, although plate stresses vary slightly. Top plate stresses seem to be on a rising trend as stress concentrations are refined, while the bottom plate is more stagnant. The relative differences in plate stress from one mesh size to the other varies between 5 % to 20 %.

Boom element size has a minor effect on the deformation, while stress is greatly affected. At small element sizes, a stress concentration emerged in the gap between leg clamp and centre hub; This is possibly an unrealistic concentration stemming from the bonded connection to a perfectly rigid leg clamp being too close to a relatively stiff centre hub. Maximal stress on the top plate is affected by the element size as well, though not as dramatically.

The modal analyses of this project were greatly affected by element number, so to conserve simulation resources the plate element size was not decreased further than 2.5 mm. Boom mesh was kept at 7 mm to avoid the erroneous stress concentration.

6.2 Goal achievement

Section 2.2 introduced the key research goals, and the results the previous Section 5 are rooted in these; Section 5.1.1 and 5.2 form a basis for comparing the structural performance of the two airframes. Section 5.1.2 describes the airframes' various modal shapes, highlighting which components are most exposed to resonance.

Key considerations and good practice has been documented throughout the thesis, mostly focused in Section 3. Section 5.1.3 discusses the effects of payloads on modal frequencies, and their importance in simulations. Sections 6.1.1 and 6.1.2 also highlight some good practice regarding element types and sizes. Section 6.2.3 briefly considers some potential improvements, though another redesign of the airframe could fuel a thesis of its own.

The next sections will directly discuss the research goals, summarise the results relevant to each, and present conclusions drawn from these.

6.2.1 Relative structural performance

Comparing the structural performance fell into two parts: Modal and static. While the static structural simulations resulted in easily comparable results, the modal analysis requires more qualitative interpretation. Quantitative results are listed in Table 11.

Section 5.1 gives considerable insight into the modal properties of the FX-8 and BG-200 airframes: The BG-200 model has noticeably fewer modal frequencies up to 500 Hz, and if one is particularly generous when comparing the operating range (0 to 400 Hz), the BG-200 model stands at approximately 40 modes to the FX-8's 60. Their distributions in relation to operating frequencies might be of interest to operators and for future designs, though this requires further validation.

Figure 14 shows which modes are most affected by the design difference: Modes where e.g. legs swing appear mostly unaffected, while some of the battery mount movements (which feature considerable deformation of the plates) show clear increase in frequency from the FX-8 to BG-200 design. One consequence of the differing plate stiffnesses is that some frequency groups mix, demonstrated in the

Table 11: *Performance of BG-200 relative to FX-8.*

Specification	Difference
Airframe mass	+20 %
Boom deflection	-20 %
Top plate stress	-24 %
Bottom plate stress	-58 %
Number of modal frequencies:	
0-500 Hz	-22 %
0-400 Hz	-50 %

lowest frequencies of the FX-8 design. Some modes are also not present in the BG-200 model in this range, again linked to plate deformations.

While the BG-200 model features fewer modes, the increased stiffness has brought some of the lower-numbered modes closer to the normal operating range around 40-60 % throttle. The actual ramifications of this has not been investigated, but should be kept in mind for future studies of dynamic response.

On the static structural side, the BG-200 model performs as expected: In the specified load case, it shows a 19 % reduction in boom deflection and significantly lower maximal stresses in both top and bottom plates with 24 % and 58 % reduction respectively. Stress concentrations around the weight-saving cuts in the FX-8 plates seem to exacerbate this, although the cuts in the BG-200 top plate centres also seem to be cause of some stress concentration.

To conclude, the FX-8 plates display significantly higher stresses and lower overall stiffness. Stress concentrations hamper the FX-8 statistics in particular, although the BG-200 bottom plate is also affected by the cutouts at its centre. Modal frequency analyses show a noticeable increase in stiffness as well; The BG-200 model has far fewer modal frequencies in the range evaluated, having generally increased the frequency of all vibration modes.

6.2.2 Key workflow considerations

Section 3 gives a general overview of the simulation workflow. It highlights the core considerations, and proposes some good practices regarding these. Beyond this, simulations performed for this project also investigated two subjects for consideration: Payload effects on modal simulations, and the effect element types in general.

Results from Section 5.1.3 (Figure 17) indicate that payload generally has a minor effect on most modal frequencies: With a large payload frequencies decreased by approximately 5–10 %, although one of the lowest modes saw a dramatic decrease of 30 %. Varying payload mass also varied the effect on modal frequencies, however; To conserve simulation resources, it might be advisable to simply ignore these effects and rather keep them in mind when analysing modal shapes. If one recognises modes displaying translation of the core structure (in these simulations, this only occurred vertically), one can anticipate that their frequencies may vary drastically when payloads are connected. Alternatively, one can do the reverse and run simulations with the maximal intended payload.

Element types have already been studied in previous works, but this project also included a cursory comparison of two element types for carbon fibre components. Section 6.1.1 already listed the results: The choice of element type is demonstrated to have a significant effect on results, and should be a key consideration for any similar simulations. Quadratic elements are often recommended for problems involving bending, although one should always be aware of the different pitfalls related to different element types.

Mesh size was also briefly discussed in Section 6.1.2. This features a possibly erroneous stress concentration in the booms, between the assumed-rigid leg clamps and the centre hub, highlighting the importance of mesh size and control.

6.2.3 Critical components and improvements

From the stress analysis (Section 5.2), it is clear that the booms are subject to the highest loads during hover, concentrated near the connection point to the plates. Some of the lowest-frequency modes also feature bending of the booms (Section 5.1.2); One can infer that the boom design is crucial to the airframe, and that modifications to these could drastically affect both modal frequencies as well as overall stiffness. Production of the current booms is however quite efficient; Such aspects would require consideration when assessing potential boom design changes.

While still discussing stresses: Both the FX-8 and BG-200 showed signs of stress concentration around the cutouts in their plates (Figure 16). The centre cutouts differ between top and bottom plates, and the top plate version appears to distribute stresses far more evenly; While the bottom plates' design has six evenly distributed spokes, the top plates' features eight spokes oriented along the boom directions. Modifying cutouts to better align with stress distribution appears to have a significant effect.

BG-200 plates also appear to suffer less stress than the FX-8 versions. If one wanted to optimise for weight reduction, it stands to reason that one could make the BG-200 plates thinner until they reach the levels of stress visible in the FX-8 plates. More extreme modifications, e.g. abandoning the circular centre hub and using a cross-shaped core might also give better utilisation of the material.

While the battery mount "flaps" on the top plate do not seem critical wrt. stresses, they feature prominently in several modal shapes. Currently, batteries are stacked into two packets each containing two batteries. One could possibly improve vibration response by spreading the batteries out over four separate areas, either overlapping the booms' distribution or not. Although this could effectively eliminate a vibration mode, it would also affect frequencies for boom deflection modes, and possibly more.

6.3 Future opportunities

Results from this work facilitate future improvements to the drone airframes. Projects aiming to assess the relative performance of future design changes and improvements could easily follow a similar workflow as shown in this thesis, and potentially compare results to the basis formed by its relative study. While some cursory recommendations for future improvements are given in Section 6.2.3, design changes should be performed with care; There is considerable potential for a future study to design and evaluate a multitude of relevant improvements.

A dynamic response analysis could further improve the knowledge of the airframe structures. This would ideally entail experimental measurement of propulsion vibrations, thus giving a better indication of the airframes' actual excitation frequencies and a more relevant search range for modal analyses.

If experimental evaluation of the drone designs is a subject, one could also attempt to compare the results of this thesis to the true response of the airframes. There would potentially be great differences due to the model assumptions and simplifications, though hopefully the relative values would be reasonably close. Such physical testing could form the basis of more thorough benchmarks of the drones, and allow for more absolute analysis as opposed to the relative nature of this thesis—though material information may be of greater import for such a study.

References

- [1] *30mm(27mm) Woven Finish Carbon Fibre Tube*. EasyComposites. URL: <https://www.easycomposites.co.uk/#!/cured-carbon-fibre-products/carbon-fibre-tube/woven-finish-carbon-fibre-tube/glossy-3k-woven-finish-30mm-27mm.html> (visited on 12/03/2019).
- [2] ANSYS. *ANSYS Composite PrepPost User's Guide*. Hosted by SHARCNET: https://www.sharcnet.ca/Software/Ansys/16.2.3/en-us/help/acp_ug/acp_book.html. SAS IP, Inc. 2016.
- [3] ANSYS. *ANSYS User Manual*. Hosted by SHARCNET: <https://www.sharcnet.ca/Software/Ansys/17.0/>. NOTE: The source is most accessible through Google's site search feature. E.g.: "site:sharcnet.ca Element Types". SAS IP, Inc. 2017.
- [4] David Bolek. 'Simplification methods for reducing computational effort in mechanical analysis'. Bachelor's Thesis. Saimaa University of Applied Sciences, 2018.
- [5] *Composite Materials Handbook Volume 2: Polymer Matrix Composites Materials Properties*. MIL-HDBK-17-2E. U.S. Department of Defense. 1999.
- [6] Robert D. Cook et al. *Concepts and Applications of Finite Element Analysis, 4th Edition*. 4th ed. Wiley, Oct. 2001. ISBN: 0471356050.
- [7] eFunda. *Classical Laminate Theory*. http://www.efunda.com/formulae/solid_mechanics/composites/comp_laminate.cfm. 2017. (Visited on 23/05/2019).
- [8] *FDM Nylon 12: A Strong Fatigue Resistant 3D Printing Material*. Stratasys. URL: <https://www.stratasys.com/materials/search/fdm-nylon-12> (visited on 24/05/2019).
- [9] S.D. Green et al. 'Mechanical modelling of 3D woven composites considering realistic unit cell geometry'. In: *Composite Structures* 118 (2014), pp. 284–293. ISSN: 0263-8223. DOI: <https://doi.org/10.1016/j.compstruct.2014.07.005>.
- [10] Steven Hale. *Will Poorly-Shaped Elements Really Affect My Solution?* CAE Associates. 2015. URL: <https://caeai.com/blog/will-poorly-shaped-elements-really-affect-my-solution> (visited on 24/05/2019).

- [11] *High Strength Carbon Fibre Sheet Specifications*. EasyComposites. URL: <https://www.easycomposites.co.uk/#!/cured-carbon-fibre-products/rigid-carbon-fibre-sheet/High-Strength-Carbon-Fibre-Sheet.html> (visited on 12/03/2019).
- [12] Robert M. Jones. *Mechanics of Composite Materials*. 2nd. Taylor & Francis, Inc., 1999.
- [13] Hossein Rahmani et al. ‘Mechanical Properties of Carbon Fiber/Epoxy Composites: Effects of Number of Plies, Fiber Contents, and Angle-Ply Layers’. In: *Polymer Engineering and Science* 54 (Nov. 2014). DOI: 10.1002/pen.23820.
- [14] Jonathan Shewchuk. ‘What Is a Good Linear Finite Element? — Interpolation, Conditioning, Anisotropy, and Quality Measures’. In: *Proceedings of the 11th International Meshing Roundtable* 73 (Sept. 2002).
- [15] Łukasz Skotny. *Symmetry in FEA may be dangerous*. Enterfea. 2017. URL: <https://enterfea.com/symmetry-fea-dangerous/> (visited on 12/06/2019).
- [16] *Typical Properties of Carbon Fiber*. Mitsubishi Rayon Co. LTD. Pyrofil Department. 2013. URL: https://system.eu2.netsuite.com/core/media/media.nl?id=79930&c=3937524&h=18efb53b777c00288e0c&_xt=.pdf (visited on 12/03/2019).
- [17] Jon Verbeke and S Debruyne. ‘Vibration analysis of a UAV multirotor frame’. In: *International Conference on Noise and Vibration Engineering*. Sept. 2016.
- [18] *Zoltek PX35 Commercial Carbon Fiber*. Zoltek Toray Group. URL: https://zoltek.com/wp-content/uploads/2018/02/2018_PX35-Brochure_FINAL.pdf (visited on 12/03/2019).